

# Processing of ERT data from Stabilised Columns

Inversion of cylindrical ERT data of jet grouting  
stabilised columns by using AarhusInv

**Mårten Petersson**

**Master of Science Thesis 30HP**  
ISRN LUTVDG(TVTG-5181)/1-64/(2023)

**Engineering geology**  
Faculty of Engineering  
Lund university



# Processing of ERT data from Stabilised Columns

Inversion of cylindrical ERT data of jet grouting stabilised  
columns by using AarhusInv

Mårten Petersson



**LUND**  
UNIVERSITY

THESIS

Submitted to the Division of Engineering Geology, Faculty of Engineering, Lund University in  
Partial Fulfilment of the Requirements for the Degree of Master of Science in Civil  
Engineering.

Lund 2023

Cover picture: Mårten Petersson

Lund University, Faculty of Engineering  
Division of Engineering Geology

Processing of ERT data of Stabilised Columns

- Inversion of cylindrical ERT data of JET grouting stabilised columns by using AarhusInv

Bearbetning av ERT-data från stabiliserandekolumner

- Inversion av cylindrisk ERT-data från jet-stabiliserade pelare med hjälp av AarhusInv

Author: Petersson, Mårten

Supervisors: Martin, Tina (Supervisor); Dahlin, Torleif (Assistant Supervisor)

Examiner: Rossi, Matteo

ISNR LUTVDG/(TVTG-5181)/1-64/(2023)

Keywords: inversion, ERT, quality control, jet grouting, aarhusinv

Language: English

The work is performed in collaboration with Lunds Tekniska Högskola (LTH)'s

Digital edition Lund 2023

# Abstract

Modern construction sites have high demands on soil conditions, resulting in geotechnical challenges that can be solved using soil stabilisation techniques. The reliability of these techniques is tested using different quality assurance methods. One of the most common ground-stabilizing methods is jet injection. This method involves mixing the in-situ soil with cement slurry, which is then injected with a high-pressure jet to create a ground stabilising column. To ensure that the jet grouted columns meet the designed loads, quality control methods are necessary. One critical geometric property to be controlled in jet grouted columns is the radius, as high-pressure injection can lead to significant variations with depth.

The purpose of this study was to test an alternative quality assurance method by using electrical resistivity tomography (ERT). ERT has shown potential as a quality assurance method for jet columns, but the handling of the measured data needed to be improved and handle in a program that takes the cylindrical geometry to account.

In this study, synthetic ERT data was generated and processed, simulating different kind of jet grouted columns. In addition, ERT field data from a test site in Moss, Norway was processed. To interpret the measurement results, the “apparent” resistivity was converted into “true” resistivity, by considering the cylindrical geometry. The used inversion program was AarhusInv. The synthetic data series with varying cylindrical geometries were generated using forward modeling to test the program. The synthetic data sets were subjected to different levels of noise, and inversions were performed on the models with and without noise. The inversion of the synthetic and measured data was carried out using two different models: a few-ring model and a multi-ring model. The results from the inversion of the field data were compared with inversions performed on the same data using the programs Res2DInv and pyGIMLi.

The conclusion is that the ERT measurements has a potential to be used as a quality assurance method, as clear resistivity contrasts between the existing in-situ soil and the jet grouted column could be found in the inversion results. The inversion of the synthetic data series resulted in a match between both inversion models and the design geometry. The noise affected the data, the resolution reduces by the level of noise. However, no validity check was performed on the jet grouted columns as no other quality controls could be carried out on the jet grouted column.



# Sammanfattning

Dagens moderna byggande sätter höga krav på markförhållande, vilket resulterar i geotekniska utmaningar som kan åtgärdas med hjälp av olika markstabiliserade geokonstruktioner. Konstruktionernas pålitlighet testas med olika kvalitetssäkringsmetoder. En av de vanligaste markstabiliserande metoderna som används är jet-injektering. I grund och botten bygger metoden på att in situ jorden blandas med cementslurry vilken injekteras med en högtrycksstråle. Detta kan exempelvis skapa en markstabiliserande pelare, en jet-pelare. För att kunna säkerställa att jet-pelare lever upp till dimensionerande laster krävs kvalitetssäkringsmetoder. En geometrisk egenskap som är extra viktig att kontrollera hos jet-pelare är radien, då högtrycksinjekteringen kan leda till stora variationer i radien med djupet. De befintliga kvalitetssäkringsmetoderna har en del brister i praktikalitet.

Syftet med detta arbete är att titta på en alternativ kvalitetssäkringsmetod som utförs med hjälp av en ERT-mätning (electrical resistivity tomography). ERT har tidigare visat potential som kvalitetssäkringsmetod av jet-pelare, men bearbetning och tolkning av mätdata har haft en del brister. Metoden är en geofysisk undersökningsmetod som främst används för att mäta elektriska egenskaper i marken. En traditionell mätning kan utföras genom att elektroder placeras ut i marken, injicerar ström i marken och skapar ett potentialfält. Elektrodena mäter sedan potentialskillnaderna i marken vilka sedan transformeras till resistivitetsegenskaper.

I detta arbete har mätdata innehållande den ”skenbara” resistiviteten från ERT-mätningar utförda i en jet-pelare bearbetas. För att mätningarnas resultat ska kunna tolkas omvandlas den skenbara resistiviteten till ”verklig” resistivitet. Detta gjordes med ett inversionsprogram som tog hänsyn till den cylindriska geometrin. Programmet som användes var AarhusInv. För att testa programmet skapades syntetiska dataserier med hjälp av forwardmodeller med varierande cylindrisk geometri. De syntetiska dataserierna utsattes för olika nivåer av störningar. Modellerna inverterades sedan med och utan simulerade mätstörningar i programmet. Inversionen som utfördes på den syntetiska samt den uppmätta mätdata gjordes med två olika modeller, en få-ringmodell och en fler-ringmodell. Resultaten från inversionen av mätdata har jämförts med inversioner gjorda på samma data i programmen Res2DInv och pyGIMLi.

Slutsatsen är att ERT-mätningar kan användas som kvalitetssäkringsmetod då tydliga kontraster i resistivitet mellan den befintliga in situ jorden och jet-pelaren visades i inversionsresultatet. Inversionen av de syntetiska dataserierna resulterade i ett resultat där de båda inversionsmodellerna matchade den dimensionerande geometrin. Det har inte gjorts någon kontroll av validiteten hos inversionsresultaten då det inte utförts några andra kvalitetskontroller på jet-pelaren.



# Preface

I would like to thank my supervisors Tina Martin and Torleif Dahlin for helping me to complete this thesis. It would not be possible without your consultation and great knowledge and experience on the topic. I would also like to thank my examiner Matteo Rossi for your advice on how to plot the data and how to add the noise to the synthetic data. Thanks to Geosciences Dept., Aarhus University, for providing me with the license and support for AarhusInv.

I would also like to thank Aristeidis Nivorlis for helping me get started with Matlab and taught me the basics of using AarhusInv. Without your greater knowledge and computer skills this work would have been impossible.

Finally, I would like to thank Peter Jonsson for connecting me to this work and supervisors. Without your inspiring teaching in the Field Investigations Methodology course, I would not have chosen this topic.

The work was carried out within the framework of the InfraSweden2030 project “ASSERT - Assessment of soil stabilisation using electrical resistivity tomography” (Vinnova project id 2018 00649) which is funded by Vinnova, Formas, Energimyndigheten, SBUF, Trafikverket, NCC, PEAB and Keller Grundläggning.

Lund, August 2023



# Content

<b>1</b>	<b>Introduction</b>	<b>1</b>
	Purpose and aim	1
<b>2</b>	<b>Soil stabilisation</b>	<b>3</b>
	2.1 Soil stabilisation methods	3
	2.1.1 Jet grouting	4
	2.1.2 Lime-cement pillars	5
	2.2 Quality control	6
<b>3</b>	<b>Method description</b>	<b>7</b>
	3.1 Resistivity	7
	Resistivity of different materials	10
	3.1.1 Archie's law	11
	3.2 Electrical resistivity tomography	11
	3.3 Inversion	15
	3.4 AarhusInv	17
	3.5 Data & modelling	18
	3.5.1 Few-ring model	18
	3.5.2 Multi-ring model	18
	3.5.3 Synthetic data	20
	3.5.4 Measured data	22
	3.5.5 Inverted models	22
<b>4</b>	<b>Site and method description</b>	<b>24</b>
	4.1 Moss	24
	4.1.1 Method	24
	4.1.2 Processing data	26
<b>5</b>	<b>Results</b>	<b>27</b>
	5.1 Synthetic model	27
	5.1.1 Few-ring model	27
	5.1.2 Multi-ring model	31
	5.2 Measured data	34
	5.2.1 Few-ring model	34
	5.2.2 Multi-ring model	37
	5.3 Comparison of the jet grouted columns	39
<b>6</b>	<b>Discussions</b>	<b>44</b>
<b>7</b>	<b>Conclusion</b>	<b>47</b>
	7.1 Recommendations	47
<b>8</b>	<b>References</b>	<b>48</b>
	<b>Appendices</b>	



# 1 Introduction

In modern society there is an increasing need of solving geotechnical problems, such as load failure problems, deformation problems, and flow problems. Some of those problems can be solved by using geotechnical soil stabilisation methods. Jet grouted columns and lime cement pillars are two examples of soil stabilisation methods. Both methods aim to improve the physical properties of the soil by creating a subsurface column. These improvements can for example be used to increase the bearing capacity of the soil. The jet grouted column has an irregular cylindrical shape, and a lime cement pillar has a more or less cylindrical shape (Carlsten, 1996). The increasing need has driven the development of the methods forward. The development of the methods requires development of new smart quality control (QC) techniques and improvements of the existing ones (Croce, et al., 2014). To be able to check if the jet grouted columns fulfil their intended designed radius the QC is extra important.

The placement of these stabilisations is also complicating the QC since the location is beneath the surface (Dazhi, 2005). QC methods are for example, acoustics methods, drilling, load testing and excavation. A potential QC method of the jet grouted columns is by using electrical resistivity tomography (ERT). The ERT method is aiming at giving a continuous picture of the entire grouted soil volume to create a good overview (Bearce, et al., 2016). The application of this method has already been used and tested by Nilsagård & Knutsson, 2022.

Insufficient knowledge about the capacity of the soil improvements is sometimes resulting in solutions like ‘more is better’. The usage of QC techniques enables an optimisation of the volume of material that is being used for the ground improvement structures, so that a less material consuming solution can be chosen (Dazhi, 2005; Naturvårdsverket, 2023). Ground improvements structures are in most cases built up by building materials containing cement. Minimization of cement usage reduces carbon-dioxide emissions and is therefore beneficial from an environmental perspective. Furthermore, material optimization is also beneficial from a cost-effective perspective (Pädam, et al., 2021).

## **Purpose and aim**

In this thesis synthetic and measured ERT data of stabilised columns was processed and inverted. The inversion was done with the AarhusInv software that supports cylindrical geometry. The goal is to better detect both variations in the diameter and variations in resistivity of the jet grouted column and by that improve the QC.

This thesis aims to answer the following questions:

- How well is the quality of the columns reflected by the inverted models of the columns (from site documentation and reference data from other methods).
- Is it possible to use the AarhusInv software to process the cylindrical columns?
- Is any adaptation required to process existing and new single-pillar ERT data?

The thesis begins with a literature study mostly focusing on the geophysical method that is being used for QC. Subsequently literature on ground stabilisation is presented, that includes a short description of jet grouted columns as well as lime-cement pillars. The literature study is concluded with brief information about known QC methods, a description of the inversion of

direct current (DC) resistivity data and the data processing steps. The result of the literature study is presented as a theory part in chapter 2 (Soil stabilisation) and 3 (Method description).

A number of synthetic forward models with predetermined geometry were created in AarhusInv, resulting in synthetic ERT data. The synthetic data set were inverted with the same starting models as were used for the measured field data of jet grouted columns. To test the inversion program some synthetic noise of different levels was added to the data. Measured ERT data was finally inverted in the AarhusInv software with the same starting models.

Evaluation of the inversion results was done by comparing the synthetic model and the real data model based on the measured data. Results from the inverted measured data were juxtaposed with site documentation and reference data from other methods. This was the base for the discussion, conclusions, and recommendations.

## 2 Soil stabilisation

The knowledge of the soil properties is crucial before construction of any buildings, roads or other constructions. Soil stabilisation is added to increase the load bearing capacity of the ground. The loads can be human made (constructions) or caused by the force of nature. The behaviour or response of the soil depends on its physical properties and the size of the load that is being added. Some important physical properties of the soil are shear strength, compressibility, permeability and shrinkage/swelling, etc. The effects of different loads and the impact that it may have on the soil can be evaluated and analysed by geotechnical engineers. The evaluation and analyse is preventing unfavourable effects or failures of the soil to occur (Nicholson, 2015).

If the condition of the soil is insufficient a consideration of the following measures are recommended, excavation and replacement, or property improvement modifications. There are many types of ground improvement techniques that have been used to improve the geotechnical properties of the soil to match the desired engineer conditions (Nicholson, 2015). The improvements are made by altering the primary properties of the soil/ rock by modifying the physical properties (Nicholson, 2015). The purpose of these improvements could be:

- Reducing compressibility to reduce settlements
- Increasing strength to receive higher bearing capacity
- Improving durability or stability and reduce/ increase permeability

The improvements can be achieved by methods divided in three categories of modifications, (1) without adding any new material, (2) includes adding certain material or (3) by reinforcing the soil/ground material. Stabilisation of the soil can be achieved with different kinds of methods, some of these are described in 2.1 (Nicholson, 2015).

### 2.1 Soil stabilisation methods

Reinforcements of the soil as improvement can be generalized and divided into four categories (Nicholson, 2015):

- (1) mechanical modification,
- (2) hydraulic modification
- (3) physical and chemical modification
- (4) modification by inoculations, confinement, and reinforcement

Due to overlaps between different soil stabilisation methods, one method could improve more than one physical property. This can be beneficial if the soil needs more than one improvement (Nicholson, 2015).

### 2.1.1 Jet grouting

Jet grouting is an in situ soil stabilisation method that is used on different kinds of soils. The jet grouting method is creating a subsurface stabilised column by injecting grout (usually a mixture of cement, air and water) at high pressure and high velocity into the ground (Dazhi, 2005). It creates large columns of cemented material by drilling small holes into the ground, the disturbance of the surrounding soil is limited. By connecting several columns, a hydraulic barrier can be created (Bearce, et al., 2016). The technique has been under development from approximately 1970. There are three main techniques of injecting the grout. Namely; single, consisting of grout; double, consisting of air and grout; triple fluids, consisting of water, air and grout (Croce, et al., 2014).

The jet grouting uses a high-velocity fluid that is injected through a small diameter nozzle placed on a pipe. The jet grout procedure is shown in Figure 1. The jet grouting is performed by a so called “jet grouted string”. The string is built up with different numbers of inner pipes depending on the number of fluids that is being injected. At the end of the string the fluids are conveyed to an installed tool called “monitor”. The fluids are injected through one or more small diameter nozzles that are placed on the monitor. Due to the small diameter of the nozzles, the high-pressure flow of the fluid is transformed to high-speed jets. The monitor is placed at the desired depth with the help of a rotating drilling system, the drilling bit is placed on top of the monitor. The drilling is performed with a diameter slightly larger than the pipes diameter, this enables the in situ soil to rise to the surface through the gap and make space for the grout. While injecting the monitor is rotating, the rotation angle can be adjusted to create different kinds of geometries of the cross-section (Croce, et al., 2014).

The most common method is that the pipe is drilled down in the soil and when it is brought back to the surface it injects the grout. After the jet grouting is done a jet grouted column is created, that should be cylindrically shaped. There are many different possible combinations of shapes depending on the company that is performing the jet grouting (Croce, et al., 2014).

Depending on the Jet injection system the in situ soil can be partly mixed, partly replaced or full replaced (Dazhi, 2005). Some typical soil stabilisations that can be achieved by jet grouting are:

- An increased bearing capacity
- Reduction of settlements
- Provide support to excavations
- Creating water cut-offs

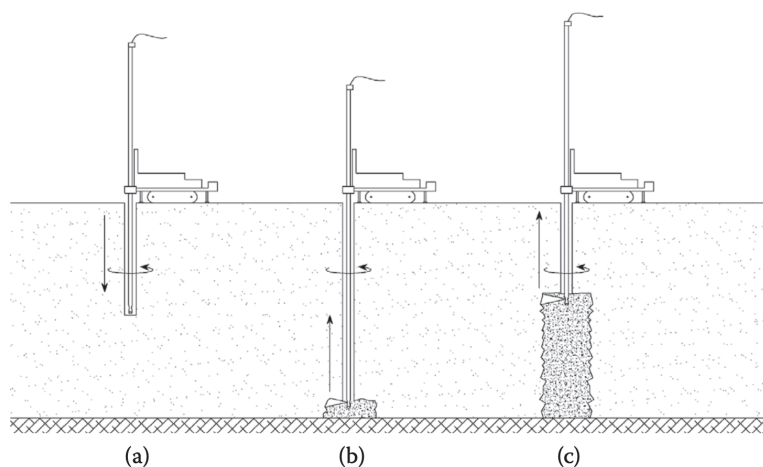


Figure 1 The jet grouting procedure, (a)- drilling, (b and c)- jet column formation (Croce, et al., 2014).

### **2.1.2 Lime-cement pillars**

Lime-cement pillars are made by using a dry-mixing technique or a wet mixing technique (Kirsch & Bell, 2013). The dry technique is used on soils with a water content of at least 20%. Cylindrical columns consisting of the cement-soil mix are created. Because of its homogenous cylindrical geometry, the columns can be called pillars (Croce, et al., 2014). When creating a lime cement pillar a shaft with a mixing tool is drilled to the desired depth. In doing so, a core of in situ material is removed and transported to the surface (Carlsten, 1996). The cement mixture is inserted into the subsurface through a rotating mixing tool (Larsson, 2006).

One difference between the jet grouted soil stabilisation method and the lime-cement method is the geometrical shape of the columns. The jet grouted columns have an irregular cylindrical shape, and the lime cement pillars have a cylindrical shape. The homogeneous geometry of the lime cement pillar is correlating with the larger size of the hole that the cement mixture is injected within. Lime cement pillars can be used for similar areas as the jet grouted columns. Two similar applications are to increase bearing capacity of the soil and reduction of settlements (Carlsten, 1996).

## 2.2 Quality control

The primary reason of control is to check if the object fulfils the requirements for its intended purpose. The quality control (QC) and quality assurance (QA) are often included in tests to ensure that the quality acuirements are fulfilled. It is important to perform QC on jet grouted columns because of its uncertainties, for example (Croce, et al., 2014):

- To ensure that the grouted materials fulfil the requirements of the installation
- To check that the installation is correctly carried out and if the equipment is working correctly
- To quantify the dimensions and the properties of the column

One of the most thorough QC that's being used is excavation of the column. In most cases it has shown that jet grouted columns have a varying diameter. This method of QC is seldomly employed and it is expensive. A measurement of a jet grouted column is shown in Figure 2 a) (Croce, et al., 2014).

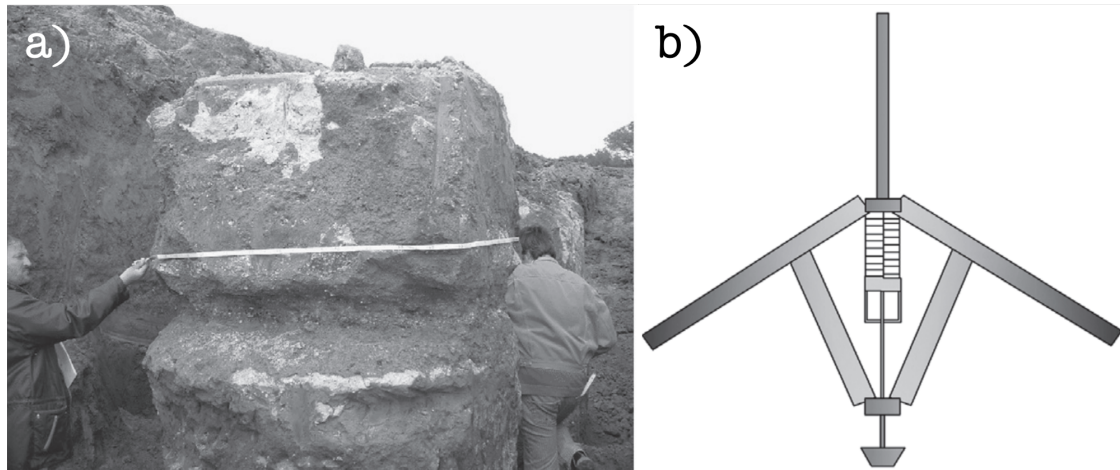


Figure 2 a) Mesurment of a excavated column, b) a calliper. (Croce, et al., 2014).

Another technique employs the calliper (Figure 2 b). It has two arms and is inserted to the freshly injected column. The two arms are connected to a hydraulic jack that is measuring variations in the spreading of the two arms. The variations can be read as the diameter of the column. The variation of the diameter is measured by moving the inserted calliper over the length of the column in the soilcrete concrete zone. The variations of the measured contrast between the soilcrete and the in situ subsurface material are translated to a diameter (Croce, et al., 2014).

The above mentioned methods of QC are direct controls but there are also some that are indirect (Croce, et al., 2014). For instance, sonic logging test and ERT method are indirect controls. The sonic logging test consists of a measurement cable that is inserted in the middle of the jet grouted hole, sonic waves is sent out from the cable. The waves travel from the center of the treated column to the untreated subsurface, then reflected. The diameter is then calculated from the sonic measurements (Croce, et al., 2014). The ERT method is described in Chapter 3.

## 3 Method description

The electrical resistivity methods are well-known geophysical methods used to measure the subsurface resistivity by inducing electrical current into the ground and measuring the potential differences (Loke, 1996). The electrical resistivity method is using direct current (DC) to measure the resistivity. The method can be used to provide information about the geology, hydrology and mineral exploration (Oldenburg, et al., 2023b).

### 3.1 Resistivity

The resistivity is defined as a conductor's ability to resist electrical current. If the conductor is homogenous and isotropic, the resistance can be calculated by using Ohm's law:

$$R = \frac{\Delta V}{I} \quad (3.1)$$

It states that the electrical current  $I$  (in ampere) flows between two points in a conductor is proportional to the electrical potential  $\Delta V$  (in voltage). The unit is in ohm ( $\Omega$ ) (Binley & Slater, 2020). The resistance,  $R$ , is directly proportional to the length, and inversely proportional to the cross-sectional area of a species. Ohm's law in a more general form can be written as:

$$J = \sigma E \quad (3.2)$$

In the equation,  $E$  (V/m) is the electrical field intensity,  $\sigma$  (in Siemens/meter = S/m) is the electrical conductivity of the conductor and  $J$  (A/m<sup>2</sup>) is the current density. In geophysical surveys, the electric field potential is measured to obtain the medium resistivity,  $\rho$  (in  $\Omega\text{m}$ ). This equals to the reciprocal of the conductivity ( $\sigma = 1/\rho$ ) (Binley & Slater, 2020). The relationship between the electric potential and the field intensity is given by the field gradient,  $\Phi$  in (Loke, 1996):

$$E = -\nabla\Phi \quad (3.3)$$

By combining Equation 3.2 and 3.3, it writes:

$$J = -\sigma\nabla\Phi \quad (3.4)$$

The current sources is almost always in the form of a point source, the elemental volume  $\Delta v$  is surrounding the current source  $I$ , which is located at  $(x_s, y_s, z_s)$  (Bearce, et al., 2016). The relationship between the current density and the current is given by:

$$\nabla J = \left(\frac{I}{\Delta v}\right) \delta(x - x_s)\delta(y - y_s)\delta(z - z_s) \quad (3.5)$$

The  $\nabla = \frac{\delta}{\delta x} + \frac{\delta}{\delta y} + \frac{\delta}{\delta z}$  and  $\delta$  is the Dirac delta function, it takes the value of 1 at the position  $x, y, z$  and is 0 everywhere else (Binley & Slater, 2020). By this the Equation 3.4 can be written as the function in Equation 3.6 which form the Poisson equation:

$$-\nabla \cdot [\sigma(x, y, z)\nabla\phi(x, y, z)] = \left(\frac{I}{\nabla V}\right) \delta(x - x_s)\delta(y - y_s)\delta(z - z_s) \quad (3.6)$$

Equation 3.6 gives the potential distribution in the ground of a point current load. This is the forward modelling problem, where the potential of an unknown subsurface that should be observed is determined, there are many ways to approach this problem. Simple analytical methods have been used for homogenous approaches like spheres or to areas with constant resistivity. For the cases with an irregular resistivity distribution, it is more common to use numerical techniques. A linear filter method is used for 1D cases where the subsurface is restricted to few horizontal layers. Finite-difference and finite-element method is used to approach 2D and 3D cases (Loke, 1996).

The simplest case is the one with a single current electrode stuck down into the ground and a homogenous subsurface. In this case the current flows radially from the electrode, with a decreasing potential in the direction away from the electrode as an equipotential surface with a hemispheric shape. The current flows perpendicular from the equipotential surface as Figure 3 displays, the potential for this one electrode is given by:

$$\Delta V = \frac{\rho I}{2\pi r} \quad (3.7)$$

With,  $r$  as the distance from the electrode. The electrode setup is in most cases containing two current electrodes, a positive current and negative current source. The potential distribution caused by a two-electrode setup is showed in Figure 4. The potential value of the two-electrode setup is calculated by Equation 3.8.

$$\Delta V = \frac{\rho I}{2\pi} \left( \frac{1}{r_A} - \frac{1}{r_B} \right) \quad (3.8)$$

Where the  $r_A$  and  $r_B$  are the distances from electrode one and two to the point in the medium. The most typical setup is the 4-electrode setup, and the potential difference of a homogenous half space is calculated by:

$$\Delta V = \frac{\rho I}{2\pi} \left( \frac{1}{r_{AM}} - \frac{1}{r_{BM}} - \frac{1}{r_{AN}} + \frac{1}{r_{BN}} \right) \quad (3.9)$$

The 4-electrode setup is shown in Figure 6. The actual measurements are carried out on an inhomogeneous soil where the subsurface has a 3-D distribution. The measurements are still made with the 4-electrode setup, by injection current to the ground in two electrodes (A and B) and then measure the potential in other two electrodes (M and N). The,  $\rho_a$  is the ‘‘apparent’’ resistivity, it is the calculated resistivity value that matches the electrode arrangement. The ‘‘apparent’’ resistivity is calculated with Equation 3.10, by the values of current ( $I$ ) and the potential value ( $\Delta V$ ).

$$\rho_a = k \frac{\Delta V}{I} \quad (3.10)$$

where,

$$k = \frac{2\pi}{\left( \frac{1}{r_{AM}} - \frac{1}{r_{BM}} - \frac{1}{r_{CN}} + \frac{1}{r_{BN}} \right)}$$

Where  $k$  is a geometric factor that is depending on the chosen 4-electrode setup. The most common used electrode setups are shown in Figure 7. An instrument are measuring the current, ( $I$ ) and the potential, ( $V$ ), the resistivity ( $R$ ) and the factor,  $k$  is calculated.

The instrument is producing values of the “apparent” resistivity,  $\frac{\Delta V}{I}$  is equal to R, this means that Equation 3.9 can be written as (Loke, 1996; Bearce, et al., 2016):

$$\rho_a = kR \tag{3.11}$$

The calculated resistivity,  $\rho_a$  is not equal to the true resistivity of the subsurface, it is an “apparent” value. The measured resistivity refers to a homogenous soil that would give the same resistivity as the measured value (Loke, 1996). The determination of the true resistivity will be accounted for in the inversion part of this chapter.

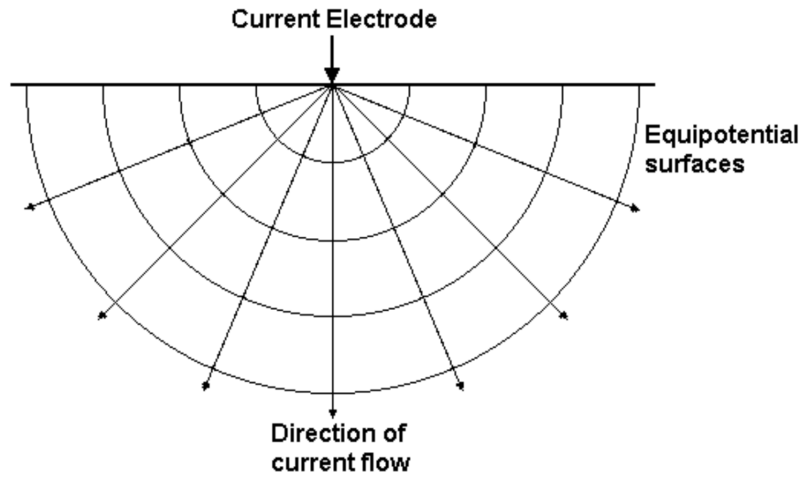


Figure 3 Simple potential distribution case with a single point current electrode (Loke, 1996).

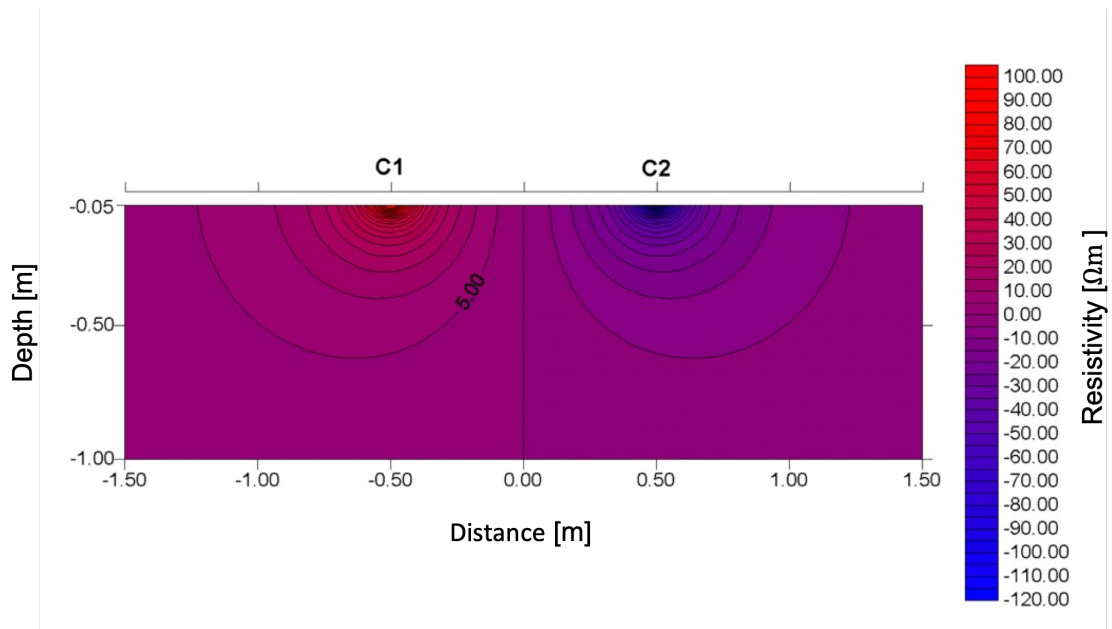


Figure 4 The color bar shows the potential distribution, V (volts) caused by a pair of current electrodes. The electrodes are placed 1 m apart with a current of 1 ampere and a homogeneous half-space with resistivity of 1  $\Omega\text{m}$ , the vertical and horizontal axis have the value meter. (Loke, 1996).

## Resistivity of different materials

Electrical current flows through material via two main mechanisms: electronic and electrolytic conduction. For electronic conduction the current flows via free electrons (i.e., in metals). The current flows via ions in the groundwater in the electrolytic method. The main mechanism in geotechnical engineering context is the electrolytic one, the electronic is more commonly used to find conductive minerals (Loke, 1996). Figure 5 gives an overview about the resistivities of different materials. For example, graphite is a better conductor than metamorphic rocks. Where the  $\rho$  stands for resistivity ( $\Omega\text{m}$ ) and the  $\sigma$  stands for conductivity with the unit mS/m (siemens per meter).

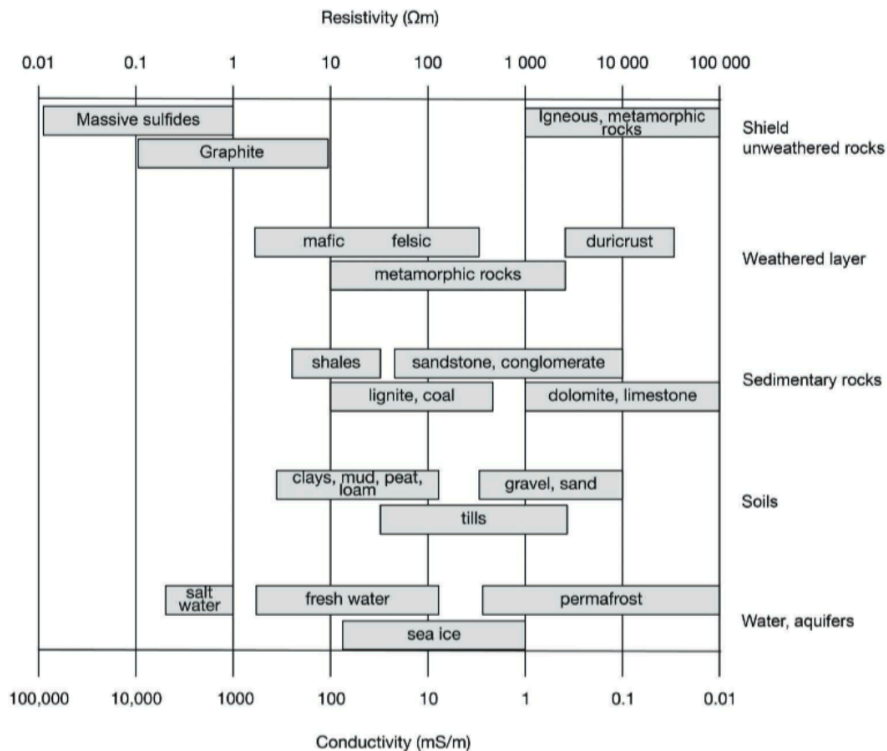


Figure 5 Resistivity of recognizable conductive materials in the ground, the resistivity and the conductivity are presented on the horizontal axis (Oldenburg, et al., 2023b).

Figure 5 shows that the resistivity can vary a lot, there is for instance a big difference in resistivity between tills, clays, sands and gravels, since they vary with a factor greater than 10. The large differences from fraction to fraction can be caused by many factors. Rock type, porosity, connectivity of the pores, the resistivity of the fluid in the soil and the metallic content affect the resistivity. This means that the measured resistivity does not always correspond to a specific soil-, rock- or fluid type. To be able to make any conclusions based on a DC resistivity measurement the knowledge about how resistivity, geological model and geotechnical parameters relate to each other is crucial (Oldenburg, et al., 2023b).

Some rocks are insulators, other can exhibit a wide range of resistivity. The conductivity of fluids in the subsurface is primarily determined by ionic conduction, whereby charged ions are responsible for transporting charges. Some porous media are insulators, but semiconductors such as sulphide or oxide minerals can be present. If all solids in a porous medium are insulators, then the electric current is restricted to ionic conduction through the electrolyte filling the pore network. This electrolytic conductivity is partly determined by the electrical conductivity of the pore-filling electrolyte, which in turn depends on factors such as ionic concentration and

temperature. Additionally, the electrical properties of the mineral surfaces may also play a role in determining the overall resistivity (Binley & Slater, 2020).

### 3.1.1 Archie's law

Archie's law is a semi-empirical relationship that describes the behaviour of electrical conductivity in a porous media, such as subsurface rocks and soils. It is a petrophysical relationship developed in the 1940s and widely used in the oil and gas industry to estimate the properties of a number of fluids (such as oil, gas, and water) in reservoir rocks. The law relates the formation factor,  $F$  which is a measure of the rock's ability to conduct electricity and the porosity,  $\phi$ .

$$F = \frac{a}{\phi^m} \quad (3.12)$$

The  $a$  and the  $m$  in the equation are the proportionality constant and the cementation exponent an empirical parameter that depends on the type of rock and fluid. Resistivity of a fully saturated rock,  $R_o$ , depends on the resistivity of the fluid,  $R_w$  (Archie, 1942):

$$R_o = F \cdot R_w \quad (3.13)$$

The resistivity of a partly saturated rock is described by the total resistivity,  $R_t$  with  $S$  being the degrees of saturation and  $n$  the saturation exponent (Archie, 1942):

$$R_t = \frac{R_o}{S_w^n} = \frac{a}{\phi^m} \cdot R_w \cdot S_w^n \quad (3.14)$$

## 3.2 Electrical resistivity tomography

A basic DC survey for measuring resistivity is by using a 4-electrodes setup, (Figure 6). The two electrodes A and B in the figure are current electrodes connected to an electrical power source. The current is transmitted to the ground, it passes through both low-resistivity and high-resistivity sections. As the current passes through parts in the ground where there is an interface, it causes local variations in electrical potential, electrical charges are built up. The voltage between electrode M and N is measured and the apparent resistivity,  $\rho_a$  is calculated. The apparent resistivity is measured if a halfspace is considered homogeneous in its electrical properties. The depth of investigation is defined as the depth where the measured voltage no longer can resolve in resistivity (Oldenburg, et al., 2023b).

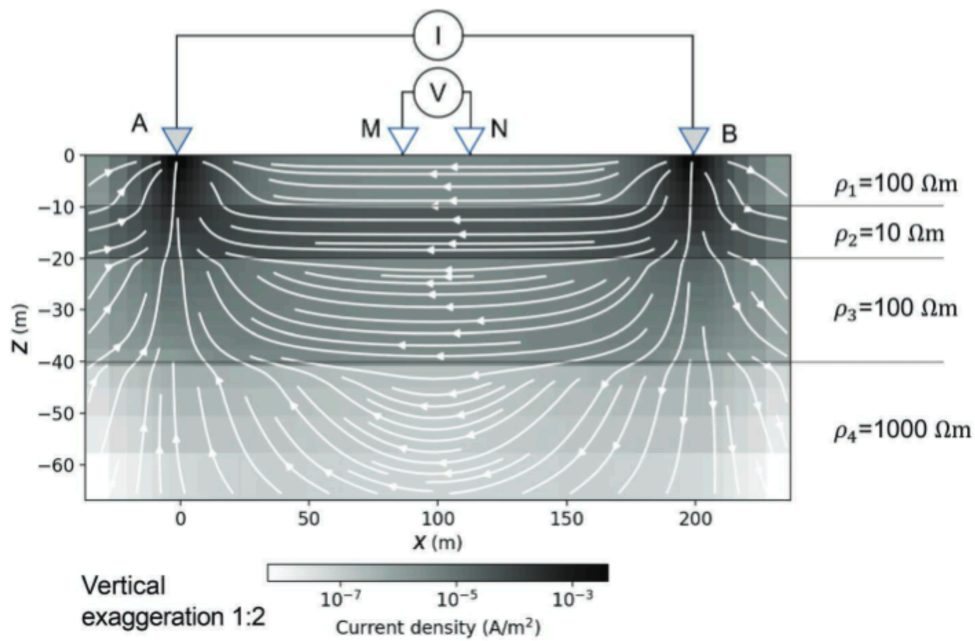


Figure 6 Theoretical 4-electrode DC resistivity setup (Oldenburg, et al., 2023b).

The electrical power source of the measurement equipment is a current transmitter that provides the setup with short rectangular pulses. By stacking the pulses, the signal-to-noise ratio can be improved. Four or more electrodes are spread out on a multichannel cable, each electrode can be used to inject current or measure voltage. In a 2D ERT setup the voltage can be measured simultaneous on several dipoles, a relay switch is used to multiplex the transmission of current and measurement channels, this speeds up the ERT measurement (Oldenburg, et al., 2023b).

The length of the array is a factor of great importance while performing a 2D ERT sounding. Measurements of a fixed array are moved laterally and the change in apparent resistivity correlates to lateral changes of the underground. A wider spacing between the electrodes is associated with greater depth of investigation. Smaller array lengths yield a shallower depth of investigation but provide a higher resolution. A measurement performed in a borehole has the same principles. The survey line is favorably perpendicular to the object of interest. Objects of interest are for example, the groundwater level, the subsurface thickness, rock structure, groundwater salinity and mineral exploration (Oldenburg, et al., 2023b).

There are different current and potential electrode arrays and many of them could be carried out by a 2D ERT system. To measure a 3D distributed array, the measurement consists of a multiple 2D ERT setup. The chosen ERT array depends on the geology and the geotechnical question of interest. The most common electrode arrays are shown in Figure 7 (Oldenburg, et al., 2023b).

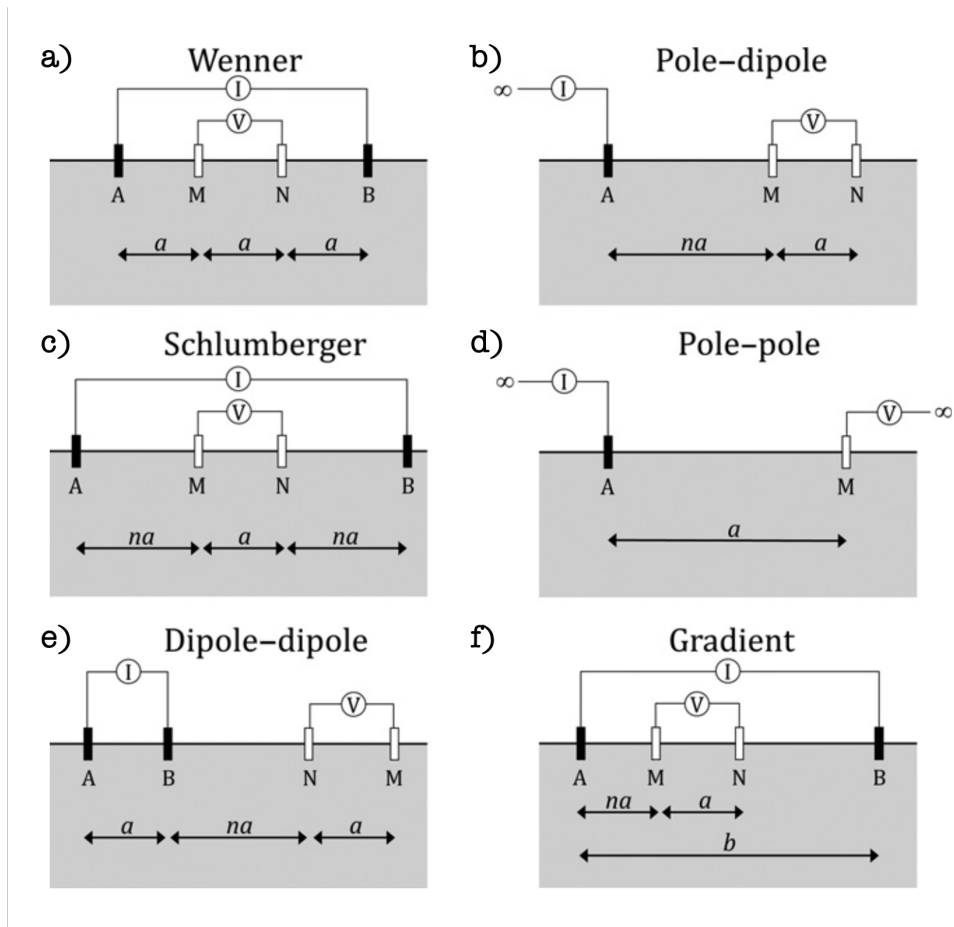


Figure 7 Most common quadrupole electrode arrays (Binley & Slater, 2020).

Each array can be moved horizontally along an electrode cable to find lateral changes in resistivity while increasing the array size one can investigate deeper. Array (a) in the figure is the Wenner array, it is one of the most common geometries. Here, the electrodes are equally spaced with a distance  $a$  apart, with the potential electrodes placed in the middle surrounded by the current electrodes. The Schlumberger (c) array is similar to the Wenner array except of the spacing of the electrodes. Here the distance between the current electrode is larger than the distance between the potential electrodes. An advantage with the Schlumberg setup is that the electrode spacing of the potential dipole,  $a$ , can change. This can increase the distance between the electrodes and the depth of investigation. In the dipole-dipole (e) array the potential and the current electrodes are separated, resulting in weaker signal. The pole-dipole (b) and the pole-pole (d) arrays are using a remote electrode or a pair of those. This increases the depth of investigation and is also a method to look at an object near the surface. The gradient (e) array in Figure 7 is an example of an multi electrode array with a quadrupole setup. The geometric factor for each array is presented in Table 1 (Binley & Slater, 2020).

To be able to perform ERT measurements in a jet grouted column or lime-cement pillar, special construction of the equipment is needed. A “special” electrode cable is used and attached during the installation, a sketch of the cable is shown in Figure 8. A denser electrode spacing is often preferable to obtain a higher resolution of the measurement. A horizontal ERT measurement is often performed with a greater spacing than in a vertical borehole measurement (Tsourlos, et al., 2007). The installation processes of a column is shown in Figure 9a. The electrode cable is placed in the centre of the column directly after the installation when the soilcrete is still wet. The lines with arrows in Figure 9b are the current flow lines and the dashed lines are the equipotential lines (Bearce, et al., 2016).

Cross-hole DC electrical survey is a method of measuring the resistivity with two electrode cables placed in two separate columns, where different holes have different electrode combinations of choice. The setup makes it possible to perform more detailed resistivity measurements of the subsurface between the boreholes (Bing & Greenhalgh, 2000) but has not been used here.

Table 1 Geometric factors for the different array geometries.

Array	Geometric factor, $K$
Wenner	$2\pi a$
Schlumberger	$\pi a n(n+1)$ or $\pi a n^2$ if $n \geq 10$
Dipole-dipole	$\pi a n(n+1)(n+2)$
Pole-dipole	$2\pi a n(n+1)$
Pole-pole	$2\pi a$
Gradient	$2\pi / \left( \left( \frac{1}{na} \right) + \left( \frac{1}{b-na} \right) + \left( \frac{1}{(n+1)a} \right) + \left( \frac{1}{b-(n+1)a} \right) \right)$

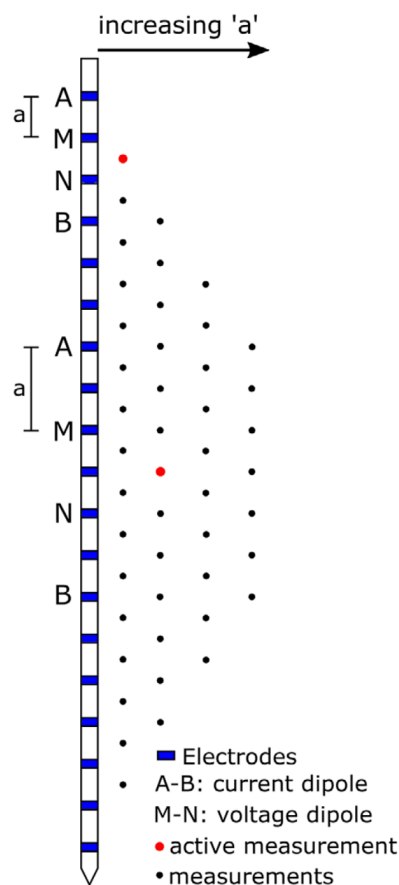


Figure 8 A sketch of an electrode cable,  $a$  is the electrode distance (Ronczka, et al., 2020).

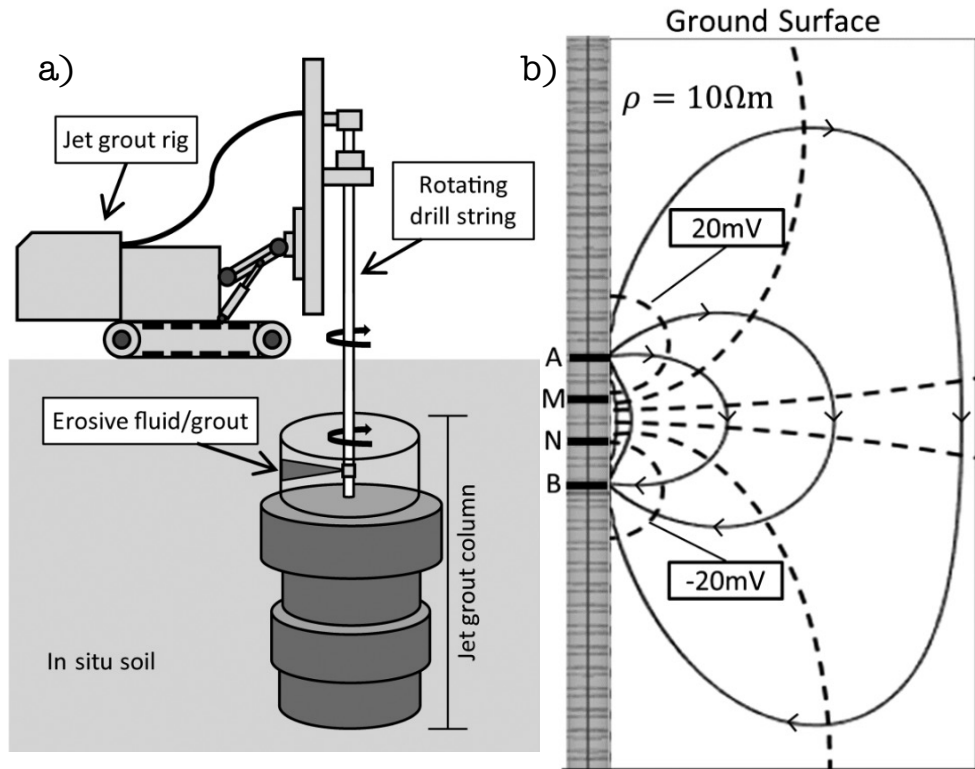


Figure 9 Illustration of, a) installation of a jet grouted column, b) ERT measurement of a single borehole (Bearce, et al., 2016).

### 3.3 Inversion

Resistivity data is measured as apparent resistivity and then visualized as sounding curves or pseudosections. A pseudosection is a two-dimensional map that shows the resistivity or conductivity distribution in a plane perpendicular to the survey line. The sections are obtained by plotting the apparent resistivity or conductivity values measured at different electrode spacings and positions (Loke, 1996). The pseudosection makes it possible to check the quality of the data and filter bad data points.

Since the pseudosections visualize the apparent resistivity, an inversion could be used to get an estimation of the true resistivities distribution. Inversion is a computational process that aims to find a model that can explain the data. The inverse results are not unique, many different inverse models can fit the data. This entails in uncertainties while interpreting the results (Binley & Slater, 2020). The depth of investigation in inversion theory is the depth range in the subsurface that can be reliably resolved by the inversion process. Inversion results is improved by incorporating prior knowledge such as layers, background resistivity and physical properties (Loke, 1996).

The inversion is performed by creating a model of the subsurface that gives a similar response as the measured apparent resistivities. In the model a section of the subsurface is presented as a mathematical idealization. The model is created based on physical quantities of interest, the quantities are estimated by using the measured data. The inversion process is underpinned by the forward model, which describes the relationship between the subsurface properties and the observed geophysical data. Inversion can be described as the reverse action of the forward model, where the goal is to estimate the subsurface properties based on the observed data (Binley & Slater, 2020). An inversion program creates an estimated model close to reality within acceptable limits of deviations from the measured data. By using an iterative process, the difference between

the model response and the observed data can be reduced (Loke, 1996). Geophysical problems are often non-linear and undetermined. This results in more complex and advanced solving techniques than a linear problem (Binley & Slater, 2020). An iterative inversion workflow scheme is shown in Figure 10.

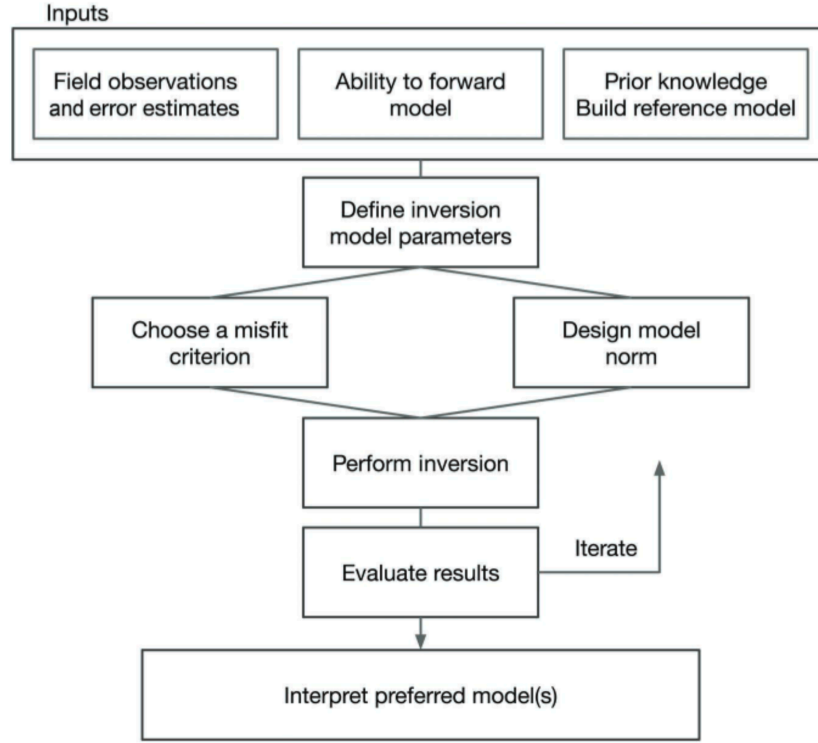


Figure 10 An iterative inversion workflow scheme (Binley & Slater, 2020).

There are three main components in setting up the inverse problem: field observations and error estimations; ability to forward model; prior knowledge to build a reference model. Geophysicists are responsible for assembling the physical data and utilizing it to carry out forward modeling (Binley & Slater, 2020).

The measured data can be written as a column vector  $\mathbf{y}$ :

$$\mathbf{y} = \begin{bmatrix} y_1 \\ y_2 \\ \dots \\ y_m \end{bmatrix} \quad (3.15)$$

The calculated model response  $\mathbf{f}$  (Equation 3.16), is also written as vector. The index  $m$  stands for the number of measurements (Loke, 1996).

$$\mathbf{f} = \begin{bmatrix} f_1 \\ f_2 \\ \dots \\ f_m \end{bmatrix} \quad (3.16)$$

The difference between the measured data and the model response is calculated by the subtraction which gives the model response,  $\mathbf{g}$  a difference vector:

$$\mathbf{g} = \mathbf{y} - \mathbf{f} \quad (3.17)$$

A measure of how the measured data fit the model response can be calculated with the least square method. A residual measure describes how well the data fits the inverted model. The error,  $\mathbf{E}$  between the measured data and the model response ( $\mathbf{g}$ ) can be determined (Binley & Slater, 2020):

$$\mathbf{E} = \mathbf{g}^T \mathbf{g} = \sum_{i=1}^n \mathbf{g}_i^2 \quad (3.18)$$

The exponent ( $\mathbf{g}^T$ ) on  $\mathbf{g}$  indicate the transpose matrix. The Gauss-Newton method is commonly used to solve least squares problem to reduce the error ( $\mathbf{E}$ ) (El-Shahat, 2017; Loke, 1996):

$$\mathbf{J}^T \mathbf{J} \Delta \mathbf{q} = \mathbf{J}^T \mathbf{g} \quad (3.19)$$

$\Delta \mathbf{q}$  is the model change parameter vector and  $\mathbf{J}$  is a Jacobian matrix containing the derivations by part. The elements of the Jacobian matrix are calculated:

$$J_{ij} = \frac{\partial f_i}{\partial q_j} \quad (3.20)$$

$i$ :th is the change in the model response due to a change in the  $j$ :th model parameter. The calculated model change parameter vector ( $\Delta \mathbf{q}$ ) is finally added to the model,  $\mathbf{q}_k$ :

$$\mathbf{q}_{k+1} = \mathbf{q}_k + \Delta \mathbf{q} \quad (3.21)$$

With  $k$  as number of iterations (Loke, 1996).

### 3.4 AarhusInv

AarhusInv is a software that models and inverts geophysical data for various configurations and sources (Auken, et al., 2014). The algorithm scheme used by the program is shown in Figure 11.

AarhusInv starts with a model file that is made in a flexible format. The model file consists of a start-up model with different constraints. Then the data files are imported. When the data has been imported and structured, it is inverted by an iterative process. Finally a sensitivity analysis is done and the depth of investigation is calculated (Loke, 1996). After the depth of investigation has been calculated, the results are written into a general file format (Auken, et al., 2014).

The starting model and the data file format for the inversion were created with the help of the AarhusInv manual and some specific examples provided by AarhusInv for a single borehole inversion. A borehole has the same cylindrical geometry as a jet grouted column, hence parts of this example have been used to support the inversion (Auken, 2020).

The inversion in AarhusInv was running with a model file and a configuration file, that are needed to set up and run the inversion. Each file name ends with a three-character long extension. The first extension is related to the model file ("mod"-file). The second extension is related to the configuration file ("con"-file), and the third relates to a data file ("dcp"-file). The result from the inversion is written to an "emo"-file. A forward response is created in a similar way. The forward response can be used to create a synthetic dataset. Forward files ("fwr"-file) are created. The program has a cylindrical model for boreholes (Auken, 2020).

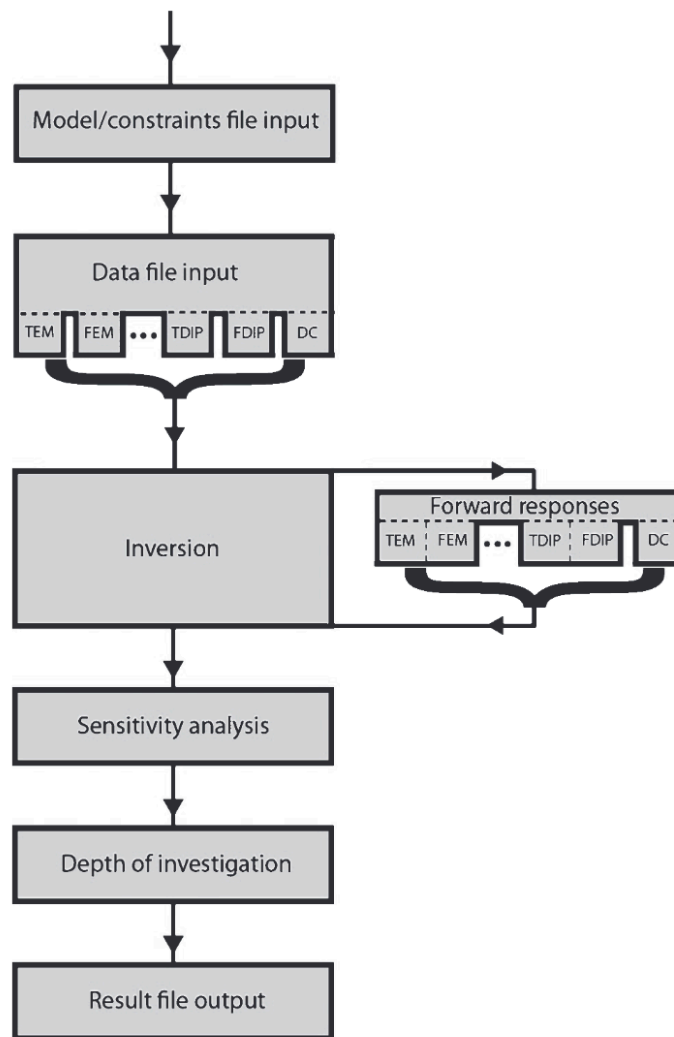


Figure 11 The general algorithm scheme of AarhusInv (Auken, et al., 2014).

## 3.5 Data & modelling

### 3.5.1 Few-ring model

The few-ring starting model is built up with three-rings, where the resistivity, radius, and thickness of every ring is free to vary. The few-ring model was used because three rings was assumed, the centre of the column, the stabilised column and the surrounding subsurface. By letting the resistivity, radius and the thickness vary the model aims to find deviations correlated to the column's geometry. The setting of the mod-file inversion is shown in Table 2. The table example is based on an inversion with a number (n) of data files. Line 7-14 contains data files.

### 3.5.2 Multi-ring model

The multi-ring starting model is built up with 18-rings, where the resistivity is free to vary but the distances from the borehole core and the thickness of each ring is fixed. By letting the resistivity vary the model aims to connect changes in resistivity to the radius by looking at each

ring. This model could possibly find deviations in resistivity of the column volume connected to the homogeneity. The setting of the mod-file inversion is shown in Table 3. The table example is based on an inversion with a number (n) of data files. Line 7-14 contains data files.

A principal ring inversion model geometry is shown in Figure 12. The figure is taken from a pyGIMLi FE mesh visualisation. In the multi-ring models there are 18 rings, and the few-ring models consist of three rings.

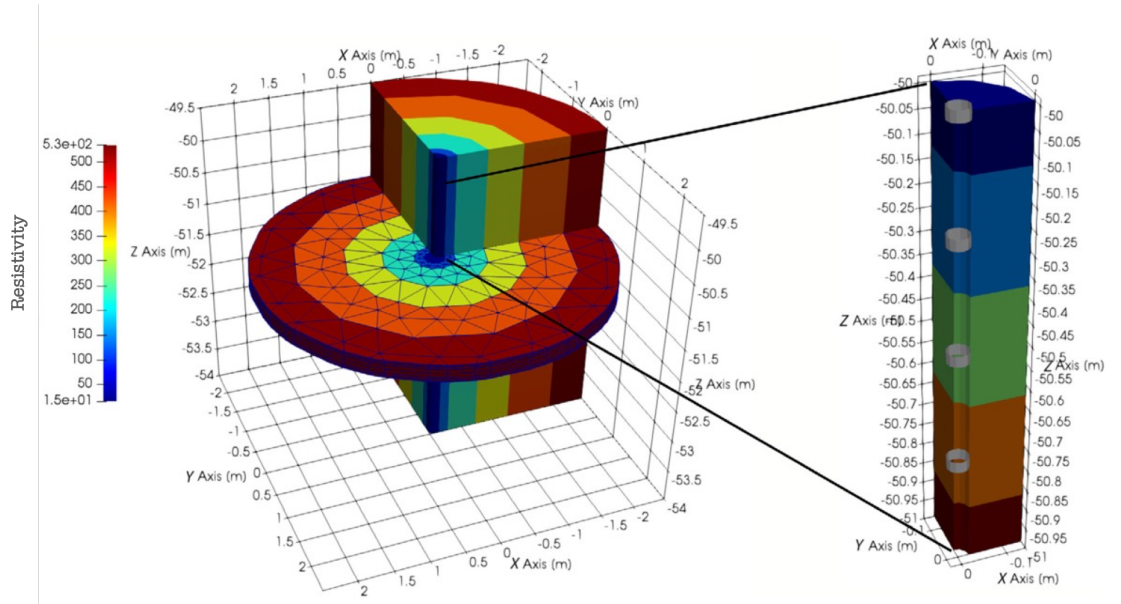


Figure 12 A visualization of the ring model, the rings are shown in the left figure and at right is the core visualized with the electrodes marked as the grey rings (Ronczka, et al., 2020).

Both the few-ring and the multi-ring model inversion are performed by a type of laterally constrained inversion (LCI). The cylindrical inversion models in AarhusInv are built up with rings placed outside of each other, it works the same way as an the layered LCI model. The principle of a layered LCI model is shown in Figure 13.

The model makes it possible to vary the thickness of the different rings. The inner ring in the few-ring model has a predetermined thickness, all the rings' radii are locked in thickness in the multi-ring model, whereas they can vary in the few-ring model. The resistivity inside the rings are free to vary in both the few-ring model and the multi-ring model (Auken, et al., 2003).

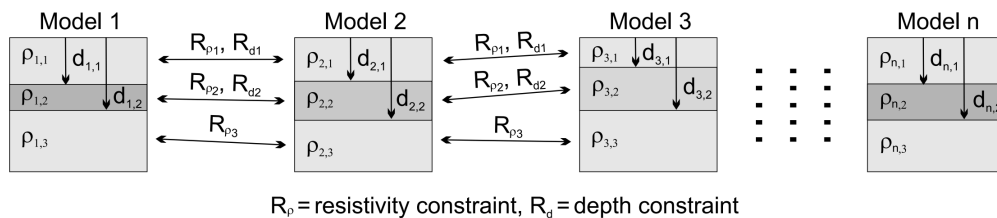


Figure 13 Laterally constrained inversion (LCI) model set-up, observe that the figure show layers stacked on top of each other, instead of rings placed beside each other as in AarhusInv (Auken, et al., 2003).

### 3.5.3 Synthetic data

To investigate the resolution of the inversion results five different models with predetermined geometries were created. For every model a forward model response was calculated. The same set of dcp-files was used for all the five forward responses. The mod-files has the same layout as the ones that has been described in the section 3.5.1 and 3.5.2 above.

The geometry is set as shown in Figure 14 (A-E). It varies by pre-set radiuses and resistivity. The geometries represent cylinders that are divided in sections with a varying radius, where at least one section has a radius of 0.6 meters. This is done to test the resolution for different possible deviations of a homogeneous cylinder.

All models consist of an inner ring (one side of the cylinder) with a radius of 0.1 meter and a resistivity of 2  $\Omega\text{m}$  (blue). The green middle ring varies in thickness but has a resistivity of 0.1  $\Omega\text{m}$ , and the red outer ring has 12  $\Omega\text{m}$ . The resistivities were chosen based on the inverted ERT data from jet grouted columns (from section 4.1 Moss). Beside of the inner blue ring, the green middle ring always has a section with a thickness of at least 0.55 meters. The models visualize the inner ring of the cylinder as the part where the grout has been injected, the middle ring as the zone where the grout is mixed with the soil and the outer ring as the surrounding in situ soil.

The first 6.5m in depth are the same for the models A, B, C. Below 6.5m depth the thickness of the green middle ring varies between 0.1m (C), 1.0m (A) and 1.4m (B). Models D and E are divided into three different sections. In model D the green middle ring is 0.55m and between 4 and 9.5 it is 0.1m. In model E the green middle ring is 0.55m, between 4 and 9.5 it is 1.4m.

The five geometries were chosen because of their simple design and to test deviations in the radius of the columns. Each of the five synthetic columns consist of at least one part with a radius of 0.6 metres and the rest of the height is testing deviations in decreases and increases of the radius. The variation of the radius is extreme, to test the program's ability to invert inhomogeneous cylinders. The extreme variation of the radius is possible on a real column. In model A, B and C there is a cylinder with the height of 6.5 metres and a radius of 0.6 metres, this part is testing how well the program is handling a homogeneous cylinder. The different resistivities of the rings is matching the resistivities of inversion results performed on jet grouted columns.

The forward response for the five models is calculated based on 27 individual files that build up a synthetic column with a height of 13 meters. The files originates from multi-gradient electrode configuration measurements containing 430 datapoints. The electrode spacing is set to 0.5 meters. Six different levels of noise are added to test the data and inverted separately. The level of noise (noise factor) is 0%, 1%, 2%, 3%, 4% and 5%. The percentage is taken from the mean and maximum value of the synthetic resistivities. The noise factor is randomly generated and normally distributed on the data points, where the noise is both positive and negative.

The synthetic factors that are being created are random and normally distributed numbers between minus one and one. The equation of these calculations reads:

$$noisy\ data = \rho_n + \left( \frac{\rho_{min} + \rho_{max}}{2} \right) \cdot \frac{[0\% \ 1\% \ 2\% \ 3\% \ 4\% \ 5\%]}{100} \cdot x(n) \quad (3.22)$$

$\rho_n$  is the resistivity of the synthetic point,  $\rho_{min}$  the minimum resistivity and  $\rho_{max}$  the maximum resistivity that is being measured by a single specific electrode.  $x(n)$  is the random factor that is being used to generate a normally distributed noise.

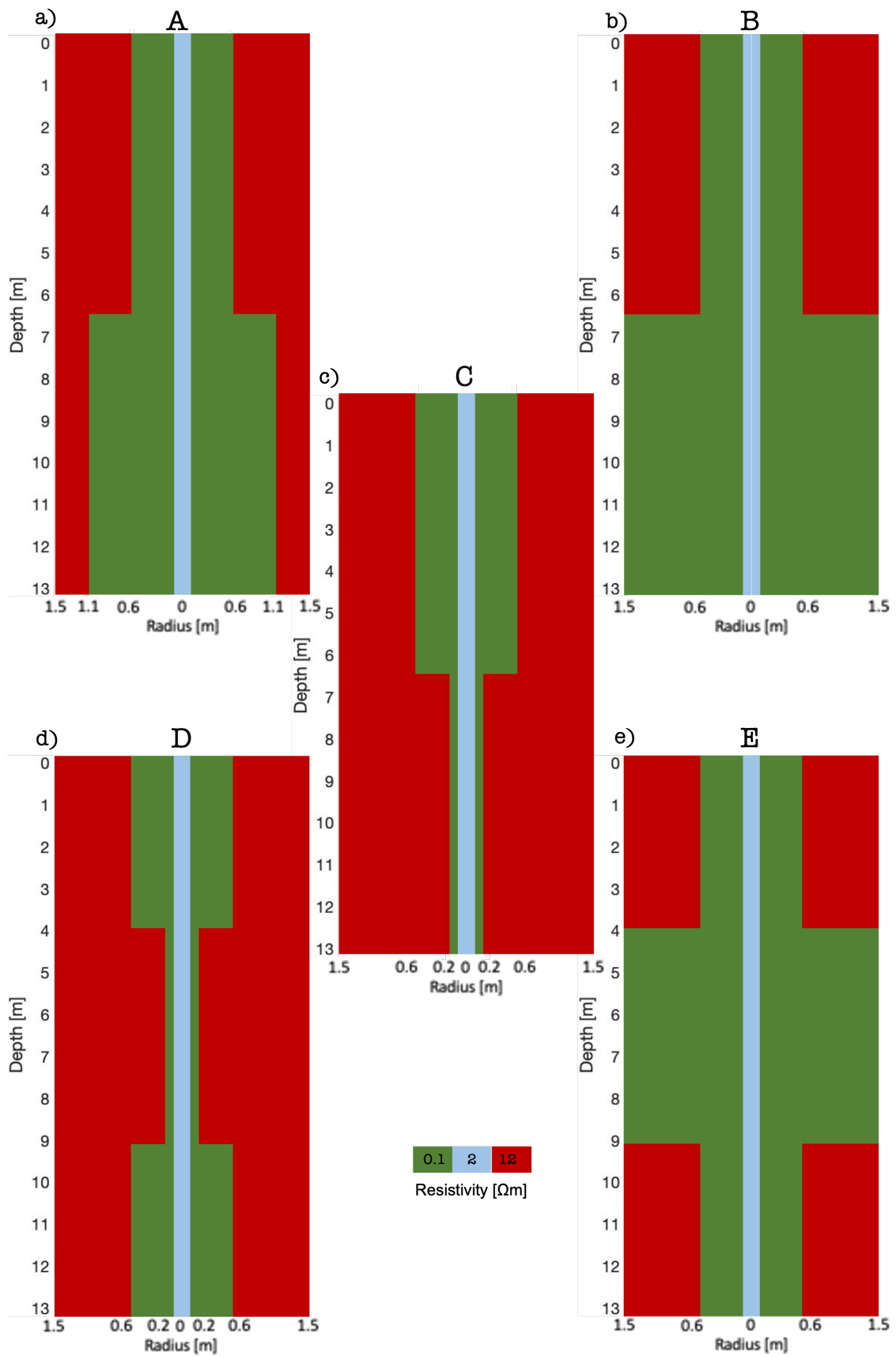


Figure 14 Synthetic models, a) model A, b) model B, c) model C, d) model D and e) model E. The horizontal scale is the radius of the column [m], and the vertical is the depth [m] of a cylinder.

### 3.5.4 Measured data

Measured resistivity data that was used for the inversion, had to be stored in dcp-files. The dcp-files that were used did originate from tx2-files. One dcp-file per depth level, which correlated with the electrode position in this case. The dcp-files and the mode-files were prepared and created by using a Matlab script. The dcp-files needed some changes in the layout. The mod-files were written with the help of the example file. The starting model geometries were chosen to match the assumed geometry of a grouted column. Some estimated resistivities was also added.

The data were inverted in two different ways, both alternatives are partly based on the single borehole example structure. The layers of a standard horizontal ERT measurement are now converted into rings. A **few-ring model** consisting of three rings, was created (see section 3.5.1). The few ring model is not only allowed to change the resistivity of each ring but also the radius and the thickness. Where the example was based on a **multi-ring model**, the structure of that model consists of 18 rings surrounding the core of the borehole (see section 3.5.2). When AarhusInv is used on a borehole, a cylindrical inversion geometry is used. The inversion results are stored in an output file (emo-file).

### 3.5.5 Inverted models

The synthetic data and the measured data have been inverted with the same starting models, both the few-ring model and the multi-ring model. The synthetic and measured data model files were the same. Every set of data resulted in two different inverted models. The maximum number of iterations was set to 50. The plots were based on the number of dcp-files multiplied with the electrode spacing to get the height of the columns. The plots that are made are based on the last inversion step.

Table 2 Settings of the AarhusInv few-ring model (mod-file).

Line	Setting
1	Name of the model.
2a	n, number of data.
2b	Constraint mode, 2 was chosen (Vertical and horizontal constraints).
3- 5 a	Model number, if n = 3 model numbers   1, 2 and 3.
3- 5 b	Parameter layout, the value 1 (General resistivity format).
3- 5 c	The name of the data file containing the expansion, for example, -.dcp.
6	50, number of integrations.
7	3, number of rings.
8- 10 a	Initial resistivities of each ring (1- 18).
8- 10 b	-1 is used. Value of, -1 is free, 0.001 can vary with the factor and 2 is fixt and cannot vary.
8- 10 c & d	Vertical & horizontal constraints.
11- 12 a	Thickness of each ring.
11- 12 b	-1 is used. Value of, -1 is free, 0.001 can vary with the factor and 2 is fixt and cannot vary.
11- 12 c & d	Vertical & horizontal constraints.
13- 14 a	Distance from center of the ring (radius).
13- 14 b	-1 is used. Value of, -1 is free, 0.001 can vary with the factor and 2 is fixt and cannot vary.
13- 14 c & d	Vertical & horizontal constraints.

Table 3 Settings of the AarhusInv multi-ring model (mod-file).

Line	Setting
1	Name of the model.
2a	n, number of data.
2b	Constraint mode, 2 was chosen (Vertical and horizontal constraints).
3- 5 a	Model number, if n = 3 model numbers   1, 2 and 3.
3- 5 b	Parameter layout, the value 1 (General resistivity format).
3- 5 c	The name of the data file containing the expansion, for example, -.dcp.
6	50, number of integrations
7	18, number of rings.
8- 25 a	Initial resistivities of each ring (1- 18).
8- 25 b	2 for first and -1 on the other lines. Value of, -1 is free, 0.001 can vary with the factor and 2 is fixt and cannot vary.
8- 25 c & d	Vertical & horizontal constraints.
26- 41 a	Thickness of each ring.
26- 41 b	0.001 is used. Value of, -1 is free, 0.001 can vary with the factor and 2 is fixt and cannot vary.
26- 41 c & d	Vertical & horizontal constraints.
42- 57 a	Distance from center of the ring (radius).
42- 57 b	-1 is used. Value of, -1 is free, 0.001 can vary with the factor and 2 is fixt and cannot vary.
42- 57 c & d	Vertical & horizontal constraints.

## 4 Site and method description

In this chapter the DC resistivity measurement setup and the information about the test site from the measured data is described.

### 4.1 Moss

The measurement data is taken from a construction site in Moss, Norway in the 2022. According to Nilsagård & Knutsson (2022) the area where the test column is placed is south-east of Moss, near the Carlberg farm. According to the geological web-map the subsurface consists of a tonalite gneiss and marine clays (Norges geologiske undersøkelse, 2023). The area where the jet grouted columns are installed consists of marine deposits (Norges geologiske undersøkelse, 2023). The ground water level is between 0.5-1.5 meters below the subsurface. The soil in the measurement area are according to Nilsagård & Knutsson (2022) consisting of clay and quick clay. A thin layer near the surface consists of topsoil but the area near the bedrock sometimes consists of sand, gravel or stones. The depth to the bedrock in the area lies between 3-27 meters, and the depth where the test column is placed is 15 meters according to Nilsagård & Knutsson (2022).

#### 4.1.1 Method

The ERT measurement is obtained from one jet grouted test column that has been measured multiple times after the grouting. Many jet grouted columns have been made in the area (Keller Geoteknikk AS, 2023). The columns are used as a soil stabilisation method for the construction of a double rail track, a tunnel, and a station. When the columns are placed in the slopes or at the foot of the slopes, the stabilization and the safety of these geotechnically weak zones is increased. The ERT measurements have been performed on a jet grouted column that was made by a double fluid system. Both cement slurry and water were injected to the subsurface. The average diameter according to the jet grouting settings should be 1.2 meter. The cement that has been used is a CEM II compound, the water to cement ratio (w/c) is 1.2 (Nilsagård & Knutsson, 2022).

The tests were performed within a master thesis in collaboration with Keller (Nilsagård & Knutsson, 2022). The measurement equipment was tested and the measurements were simulated at LTH before the tests in Moss. The equipment that they used for the measurements is listed below (Nilsagård & Knutsson, 2022).

##### Composed cable

- Four electrode cables of stainless steel with total measuring lengths of 3,5 meters (0,5 meter spacing)
- Four temperature sensors (one wire of 5 meters, two wires of 10 meters and one wire of 15 meters)
- Steel wire covered with polyurethane (20 meters length)
- Fibreglass rod (20 meters in length)
- Anchorage (Steel pipe of 1 meter in length and 4 steel nails)
- Duct tape

##### Measuring device

- ABEM Terrameter LS 2
- Temperature-logger with 4 channels
- 12-volt, 75-ampere hour battery

The composed measuring cable consisted of cables with 8 electrodes with a spacing of 0.5 meters. The cables had a length of 3.5 meters, so when the cables were put one after the other 0.5 meters apart the total length was 15.5 meters with 32 electrodes. Temperature sensors were also installed with a spacing of four meters apart, distributed over the length of the column. The temperature sensors were placed between the electrodes to avoid disturbance from the conductors, a steel wire covered in polyurethane were added to increase the tensile strength. A fiberglass rod was used to provide the composed cable with sufficiently high stiffness. All components were put together with duct tape. Figure 15 shows different components of the composed cable. Part a of the figure shows a temperature sensor, an electrode and a steel wire. Part b shows the fiberglass rod and part c shows the whole composed cable duct taped together (Nilsagård & Knutsson, 2022).

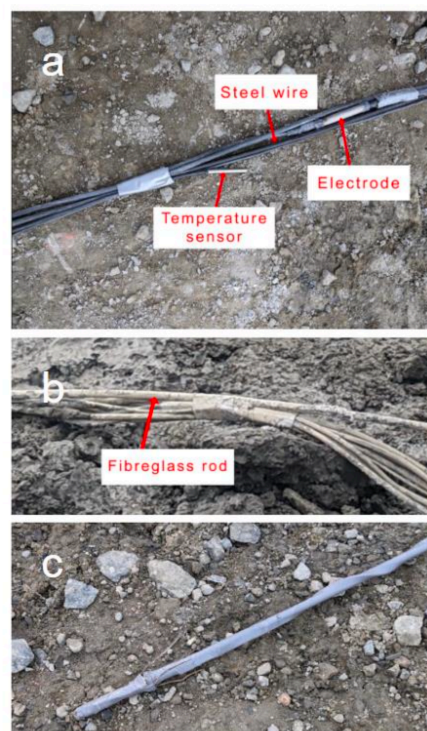


Figure 15 Composed cable for borehole ERT & temperature measurements (Nilsagård & Knutsson, 2022).

An ABEM Terrameter LS2 was used to measure the apparent resistivity of the subsurface. The data was then saved for later processing. The power source device was a 12-volt, 75-ampere hour battery. Table 3 shows the different time steps when the measurements were taken, all the ERT measurement has a multigradient electrode configuration. Temperature sensors were connected to a Comet U0141M temperature logger. The temperature was measured every 10 minutes.

The column was installed by a jet grouting machine, and directly after the installation the monitor was replaced with a hollow nozzle to make space for the composed cable. The cable was then inserted to the column in the fresh concrete. To make sure that the installation was straight inside the column, it was anchored in the bottom of the column. A detailed configuration of the measurements in Moss can be found in Nilsagård & Knutsson (2022).

The data from Nilsagård & Knutsson's (2022) are measured with a multi-gradient electrode configuration that are containing 430 datapoints. A more detailed description of the ABEM Terrameter LS2 settings is presented in their thesis. The multi-gradient array provides stable field data, since it has a good signal-to-noise ratio. Inversion models based on multi-gradient

measurements compare well to inversions performed on Wernner or dipol-dipole data. It is a good alternative for both single or multichanel measurements. The multi- gradient array is a full range survey, the array gives an improved version of the multi- gradient array with a clearer resolution of the mesured data in comparision to the original array. The full-range-gradient survey are not just performing measurements between the electrodes but the potential electrodes can be outside the curent dipole (Zhou, et al., 2020; Dahlin & Zhou, 2006).

Table 3 Dates when resistivity measurements were taken, time of curing and measurement configuration.

Occasion	Date	Time of curing [hours]
1	2022-04-06	1
2	2022-04-07	17
3	2022-04-07	26
4	2022-04-08	41
5	2022-05-09	789

#### 4.1.2 Processing data

The data from the ERT measurement was processed and inverted with the aim to find a boundary between the untreated and treated soil. The data files were processed in the software “Terrameter LS Toolbox”, which is used to export the raw data (Nilsagård & Knutsson, 2022). The inversion was done with the following programs:

- Res2DInv
- pyGIMLi
- AarhusInv

More details about the inversion done in Res2DInv and pyGIMLi is found in Nilsagård & Knutsson (2022). The inversion done in AarhusInv is done with the **few-ring model** and the **multi-ring model** in this thesis.

The relative resistivity changes were calculated by the difference between the inverted resistivities after one hour of curing and the values from a later time of curing (17h, 26h, 41h and 789h). The difference was then divided by the resistivity values from one hour of curing to calculate the percentage difference.

The residuals of each inverion is giving a value of the deviation of the inversion result and the measured data. A value of 1.0 means that the model is well fitted and a value higher is showing that there are deviations. A value below 1.0 means that the model is excessive fitted. The residuals is read as a “norm factor” in the emo-file, the norm factor of the last inversion step is used.

# 5 Results

The results will be presented in two parts, one for each type of inversion model. The models are the few-ring model and the multi-ring model. The inverted data used in the models originates from the synthetic data set and measured data. The synthetic data has been created with a forward model in AarhusInv. The measured data was sourced from a jet grouted pillar in Moss, Norway. The results of the inversion are visualised in plots for both models. The vertical axis ( $z$ ) is the depth of the borehole, the horizontal axis ( $x$ ) is the radius of the borehole. The axes are presented in metres. The used colour scale is the same for all figures. The two inversion results based on Moss data are compared with Nilsagård & Knutsson's (2022) results from their inversions in Res2DInv and pyGIMLi.

## 5.1 Synthetic model

Figure 16 and Figure 18 presents the inversion results of the synthetic data set, without noise. The five different geometric designs of the synthetic data are shown in Figure 14. The models are named A, B, C, D and E. In each of the five data sets have been affected by five levels of noise: 1%; 2%; 3%; 4%; 5%. Figure 17 and Figure 19 show model A with, 1%; 2%; 4% of noise and model D with, 2%; 4% of noise.

### 5.1.1 Few-ring model

In Figure 16 the inversion results of model A, B and E are matching the designed geometry. However, there are some negligible deviations in the scale of a few centimetres. Model C and D exhibit deviations in the inverted part when the radius is only 0.2 metre. In contrast to the designed geometry, the inverted parts of model C is growing with depth. The radius in model D grows towards the middle of the model, which forms a curved part. The deviations are around 35 cm for C and 10 cm for D. The medium resistivity section (turquoise) in the middle of all models, where the radius is 0.65 metres, has a deviation between 0 and 0.5 meters. In model C there is an increase of the resistivity towards the depth in the zone 6.5- 13 meters.

In Figure 17, the three figures pertaining to model A shows that the increasing noise level worsens the resolution and the layer boundaries are not well resolved (Figure 17 a-c). Similar result can be seen for the two models of D (Figure 17 d&e) where the increasing noise level worsens the resolution. It is shown that 4% noise makes the layers grow far away from the design geometry boundary and the result is not easy to read anymore. The geometries of Figure 17c&e do not represent the designed geometry anymore. An increasing noise level tends to make the radius overdetermined, the areas with a radius below 0.6 meters is the most affected by the noise. Both D models in Figure 17 (d, e) has an increase of the resistivity in the middle of the height. All the models in both Figure 16 and Figure 17 have a horizontal low resistivity ring near the surface that differs from the rest of the column in resistivity.

Table 4 shows the residuals of the synthetic few-ring models without noise and with 5% noise. The figures of the inversion results of the synthetic data with 5% noise are shown in the appendices. The residuals are higher for the data that has been affected by noise. The residuals with values below one are meant to have an excellent fitting between to the model response and data.

*Table 4 The data residuals of the synthetic data, based on the few-ring model inversion results.*

<b>Model - noise level</b>	<b>Residual [-]</b>
A - 0%	0.688
B - 0%	0.855
C - 0%	0.666
D - 0%	0.649
E - 0%	0.841
A - 5%	15.177
B - 5%	10.679
C - 5%	2.545
D - 5%	1.927
E - 5%	18.109

### Few-ring model, synthetic data

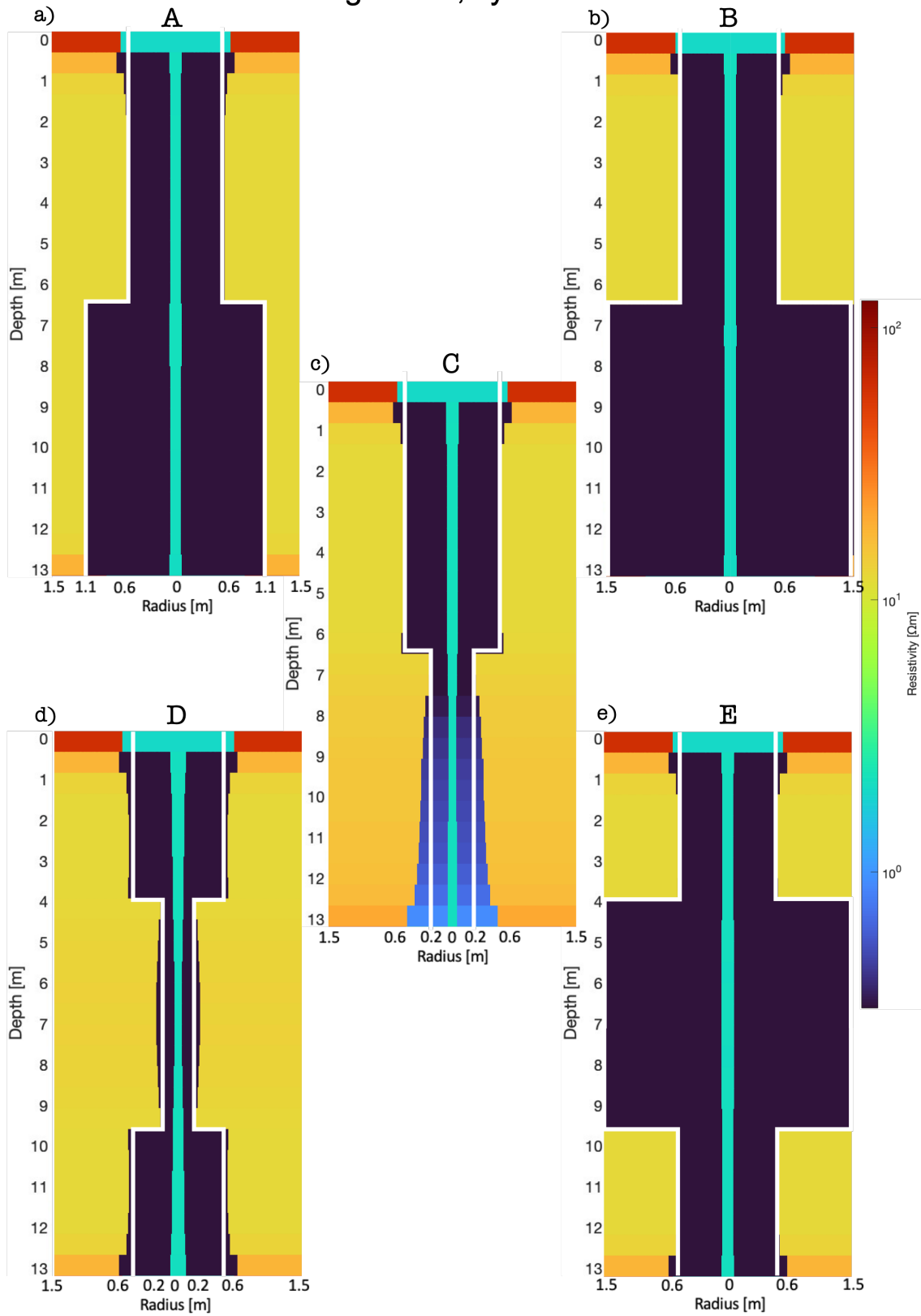


Figure 16 Few-ring model of the synthetic data. a) A, b) B, c) C, d) D and e) E are different geometric designs of the borehole. The white lines show the designed geometries (see Figure 14).

### Few-ring model, synthetic data with noise

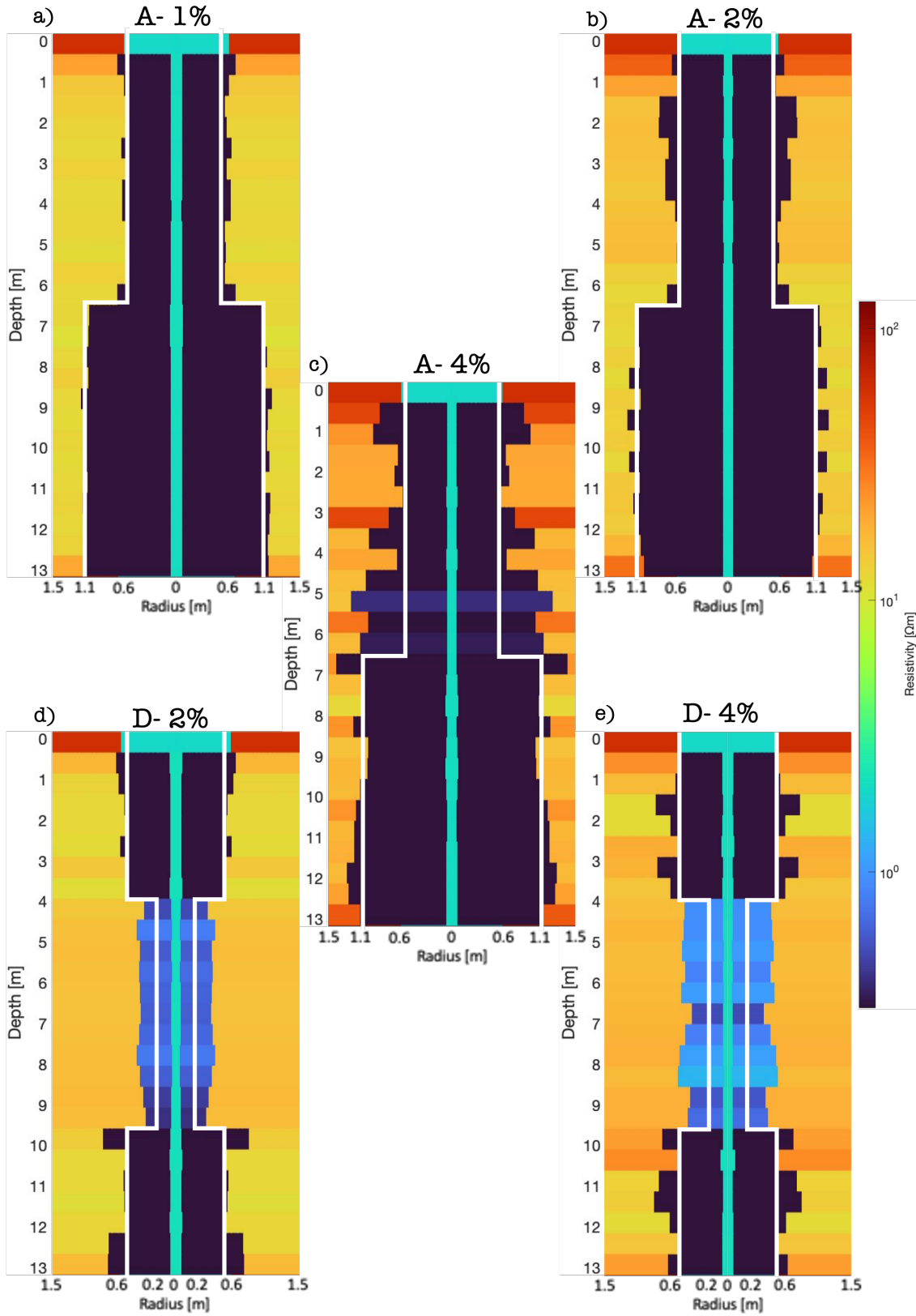


Figure 17 Few-ring model, of the synthetic data. a) A- 1%, b) a- 2%, c) A- 4%, d) D- 2% and e) D- 4% are different geometric designs of the borehole, the percentage indicates the level of noise. The white lines show the designed geometries.

### 5.1.2 Multi-ring model

In Figure 18a it can be seen that model A is matching the designed geometry. However, there is a small deviation in the bottom of the figure where there is a protruding part at the depth between 12.5 and 13 metres. Model B and E are also matching the design. Model C and D have a section between 4 and 9.5 meters where the designed radius of 0.2 meters is not recognised. The medium resistivity section (turquoise) in the middle of all multi-ring models match the design geometry better than the few-ring models.

Figure 19 shows model A with an increasing noise level in three steps. The two D figures (d,f) show a similar result, the middle part is only minor affected by the noise. The radius of the middle part between 4 and 9.5 is still not recognised. A noise level of 4% makes the inversion results unreliable. The radius of the columns tends to grow with an increasing level of noise. The inserted part in model D (see Figure 17d&e) is blurred and the resistivity is lower here than the rest of the column. All the models in both Figure 17 & 18 have a gap between 0- 0.5 meters where the column is missed and has been replaced with a high resistivity part (yellow in the Figure 17 & 18).

Table 5 shows the residuals of the synthetic multi-ring models without noise and with 5% noise. The figures of the inversion results of the synthetic data with 5% noise are shown in the appendices. The residual values are higher for the data with noise in comparison to the one without noise. The ones without added noise have higher residuals than the corresponding few-ring model.

*Table 5 The data residuals of the synthetic data, based on the multi-ring model inversion results.*

Model - noise level	Residual [-]
A - 0%	2.552
B - 0%	1.294
C - 0%	1.270
D - 0%	1.352
E - 0%	1.366
A - 5%	13.760
B - 5%	14.256
C - 5%	8.635
D - 5%	7.763
E - 5%	6.696

### Multi-ring model, synthetic data

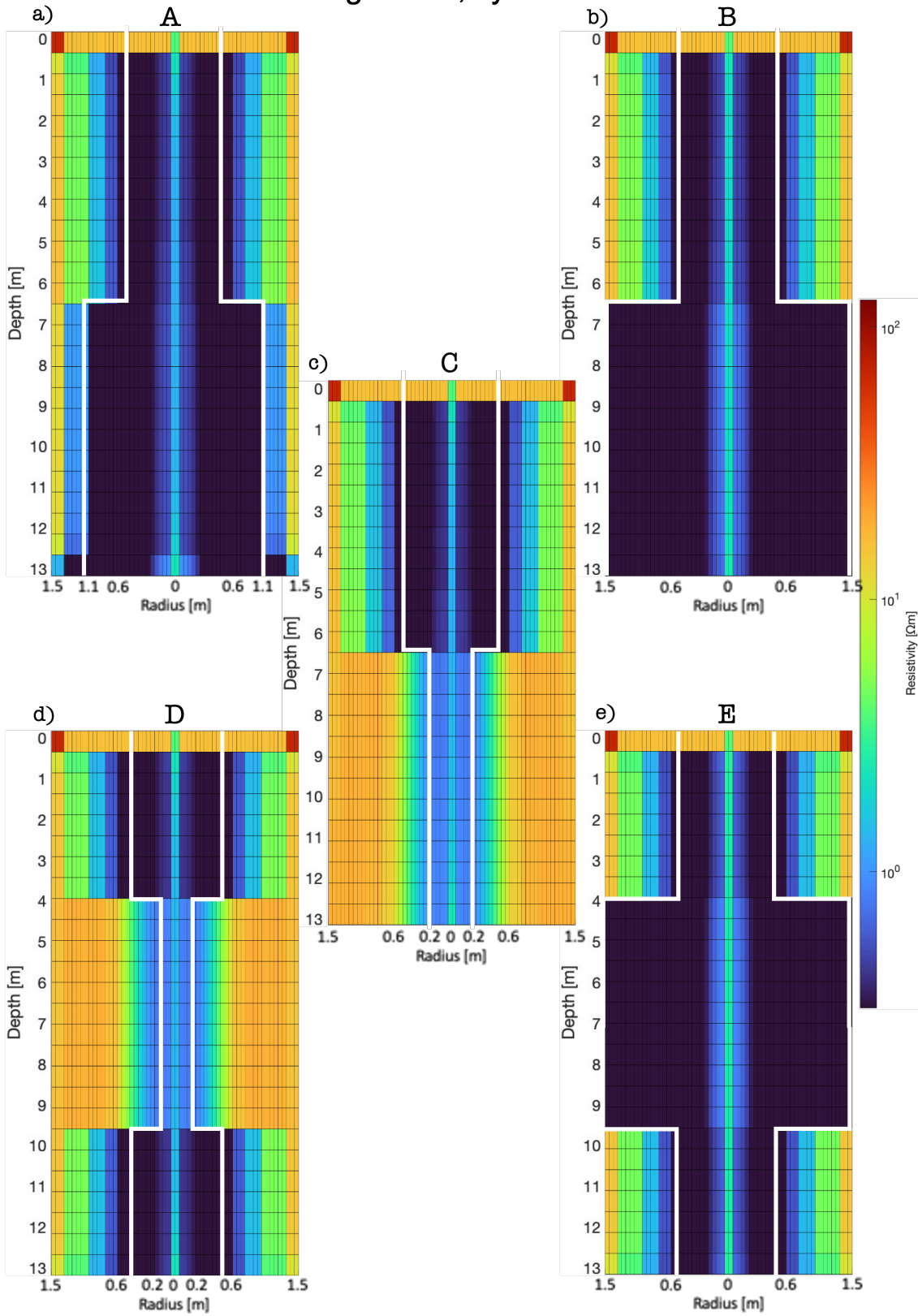


Figure 18 Multi-ring model, of the synthetic data. a) A, b) B, c) C, d) D and e) E are different geometric designs of the borehole. The white lines show the designed geometries (see Figure 14).

### Multi-ring model, synthetic data with noise

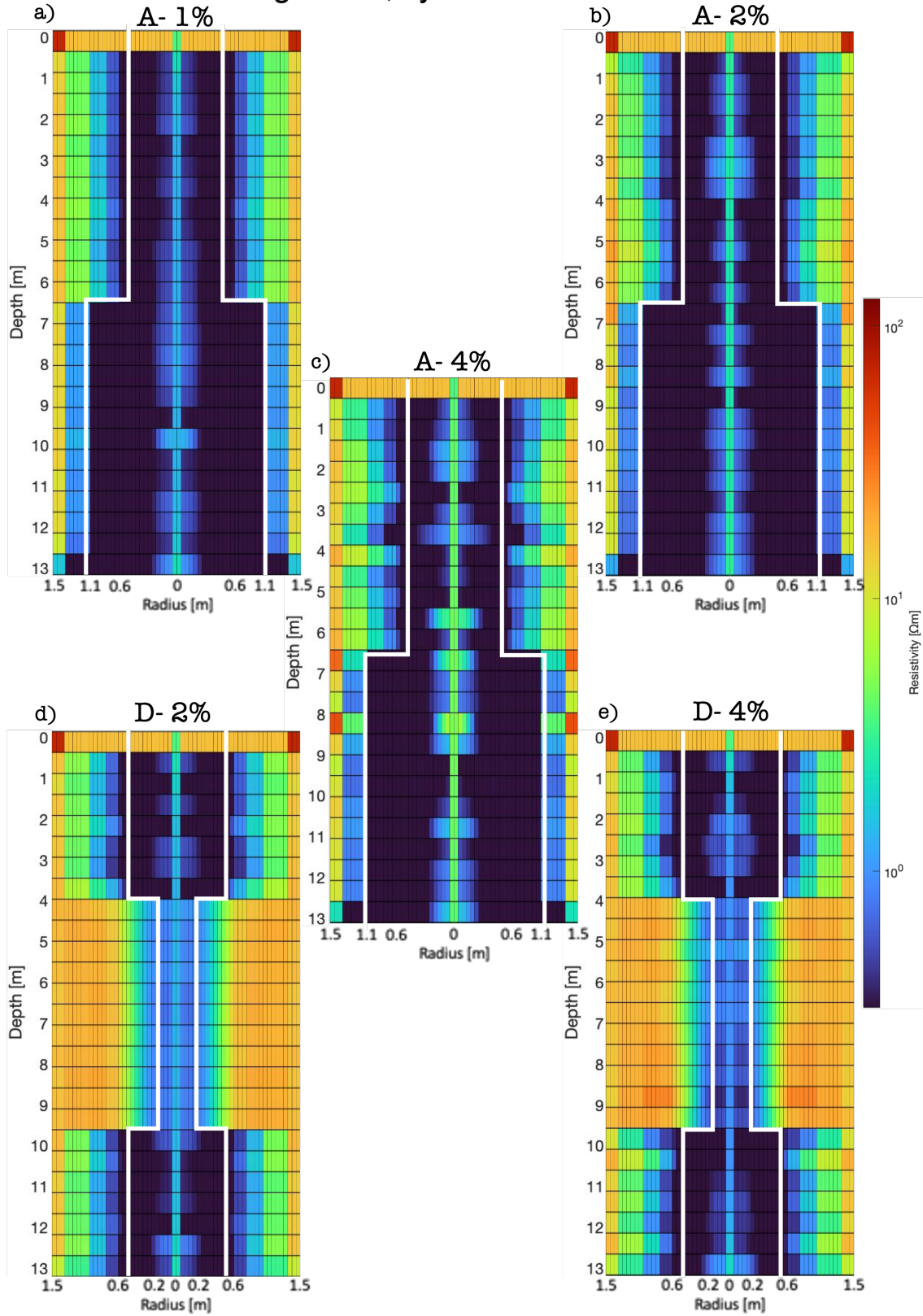


Figure 19 Multi-ring model, of the synthetic data. a) A- 1%, b) a- 2%, c) A- 4%, d) D- 2% and e) D- 4% are different geometric designs of the borehole, the percentage indicates the level of noise. The white lines show the designed geometries (see Figure 14).

## 5.2 Measured data

The inversion results based on data measured in Moss are shown in Figure 20 and Figure 22. The plots, A, B, C and D show the different measurement times after injection: The measurement in A is taken after 1 hour of curing, B after 17 hours, C after 26 hours of curing and D is taken after 41 hours of curing. The measured data from Moss is based on a multigradient configuration ERT array (see chapter 4).

### 5.2.1 Few-ring model

The few-ring inversion results from Moss are shown in Figure 20. The plots A, B, C and D are based on the same starting model. In Figure 20 the models show that the low resistive zone is mostly within 0.6 metres with occasional parts that are greater than 0.6 metres. This zone has the lowest resistivity in all four models. All the figures have a vertical part in the middle with a resistivity that is about  $2 \Omega m$  for all the models. The surrounding resistivity is in the span between 10 and  $100 \Omega m$  and is by that the most resistive zone. Model B, C, D have a low resistivity part in the bottom of the Figure 20 that is covering the hole radius (1.5 metres). Figure 20 show that the resistivity is changing through the curing process, the resistivity is the lowest in model B (17h) and highest in model D (41h). The geometry of the column is decreasing from model A (1h) in comparison to model B, C, D where the volume of the cylinder is decreased. All the models in Figure 20 have a surface disc in the span 0- 0.5 metres where the resistivity is higher than the rest of the column. The resistivity of the disc is better matching the middle cylinder. The inversion result from measurement performed after 789 hours of curing is shown in Figure 21, model E. The model fitting of the inversion is poor, the low resistivity stabilised column zone in the middle is no longer visible. The resistivity of the surrounding soil has decreased. The low resistivity core of the column is still visible, so is the 0.5 metres high resistivity at the shallow layer.

The residuals are presented in *Table 6*, the value from model B and E are much higher than the rest of the values, indicates noisier data with time.

*Table 6 The residuals of the measured data, based on the few-ring model inversion results.*

Model - hours of curing	Residual [-]
A - 1h	8.515
B - 17h	19.422
C - 26h	11.316
D - 41h	11.300
E - 789h	25.978

### Few-ring model, measured data Moss

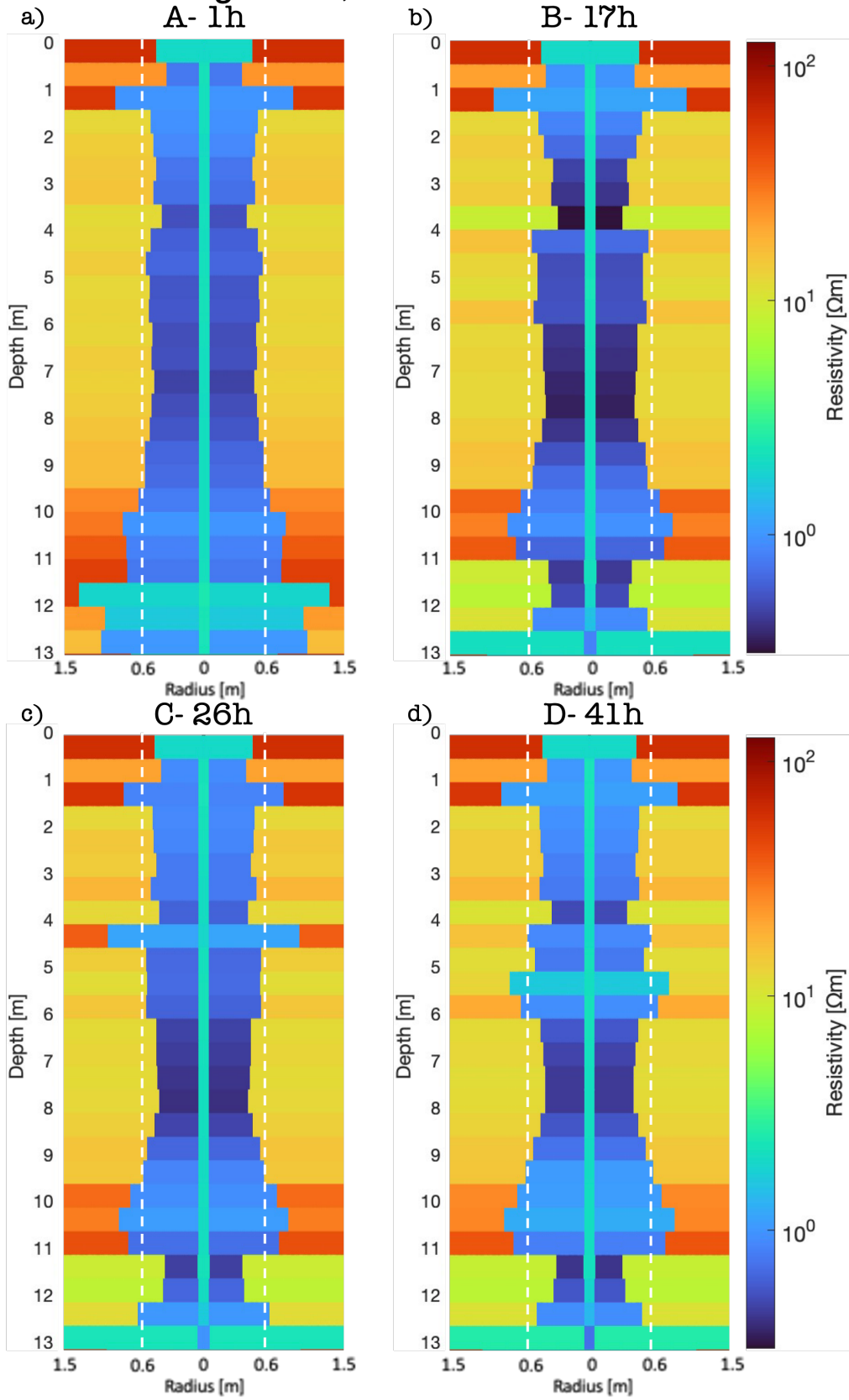


Figure 20 Few-ring model, of the data from Moss. a) A, b) B, c) C and d) D are measurements taken after different times of curing. A, 1h; B, 17h; C, 26h; D, 41h. The dashed lines show the nominal diameter.

# Few-ring model, measured data Moss

E- 789h

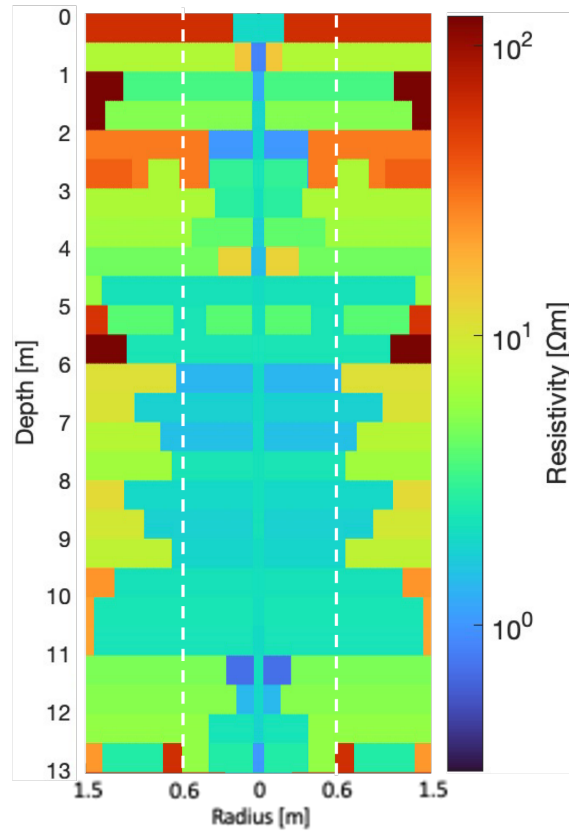


Figure 21 Few-ring model of the data from Moss. E are measurements taken after 789h of curing. The dashed lines show the nominal diameter.

### 5.2.2 Multi-ring model

In general, the multi-ring model inversion results are similar to the few-ring model results. In Figure 22, model A, B, C and D show that there is a low resistivity zone with resistivity values  $<10\Omega m$  and a radius around 0.6 metres. There are some projecting parts in the zone that are greater than 0.6 metres. All the figures have a vertical part in the middle with a resistivity that is about  $2\Omega m$  for all models. The surrounding area is similar for all the figures and shows higher resistivity. The radius of the low resistivity part in the multi-ring inversion result (Figure 22) compared to the few-ring inversion result (Figure 20) is similar but the boundary zone between the low zone and the high resistivity is not as sharp as in the multi-ring there is a transition zone. All of the models in Figure 22 have a high resistivity ring near the surface between 0- 0.5 metres. The resistivity of the column in Figure 22 model B & C are lower than in model A & D. The geometry of the column in Figure 22 model A, B, C and D is similar. The inversion result from measurement performed after 789 hours of curing is shown in Figure 23, model E. The resolution of the inversion is bad, the low resistivity stabilised column zone in the middle is no longer visible. The resistivity of the surrounding soil has decreased. The low resistivity core of the column is still visible with higher resistivity than before, so is the 0.5 metres high resistivity near surface layer.

The residuals the are presented in Table 7. the value from model D and E are much higher than the rest of the values.

Table 7 The data residuals of the measured data, based on the multi-ring model inversion results.

Model - hours of curing	Residual [-]
A - 1h	11.050
B - 17h	11.300
C - 26h	10.969
D - 41h	25.978
E - 789h	26.003

### Multi-ring model, measured data Moss

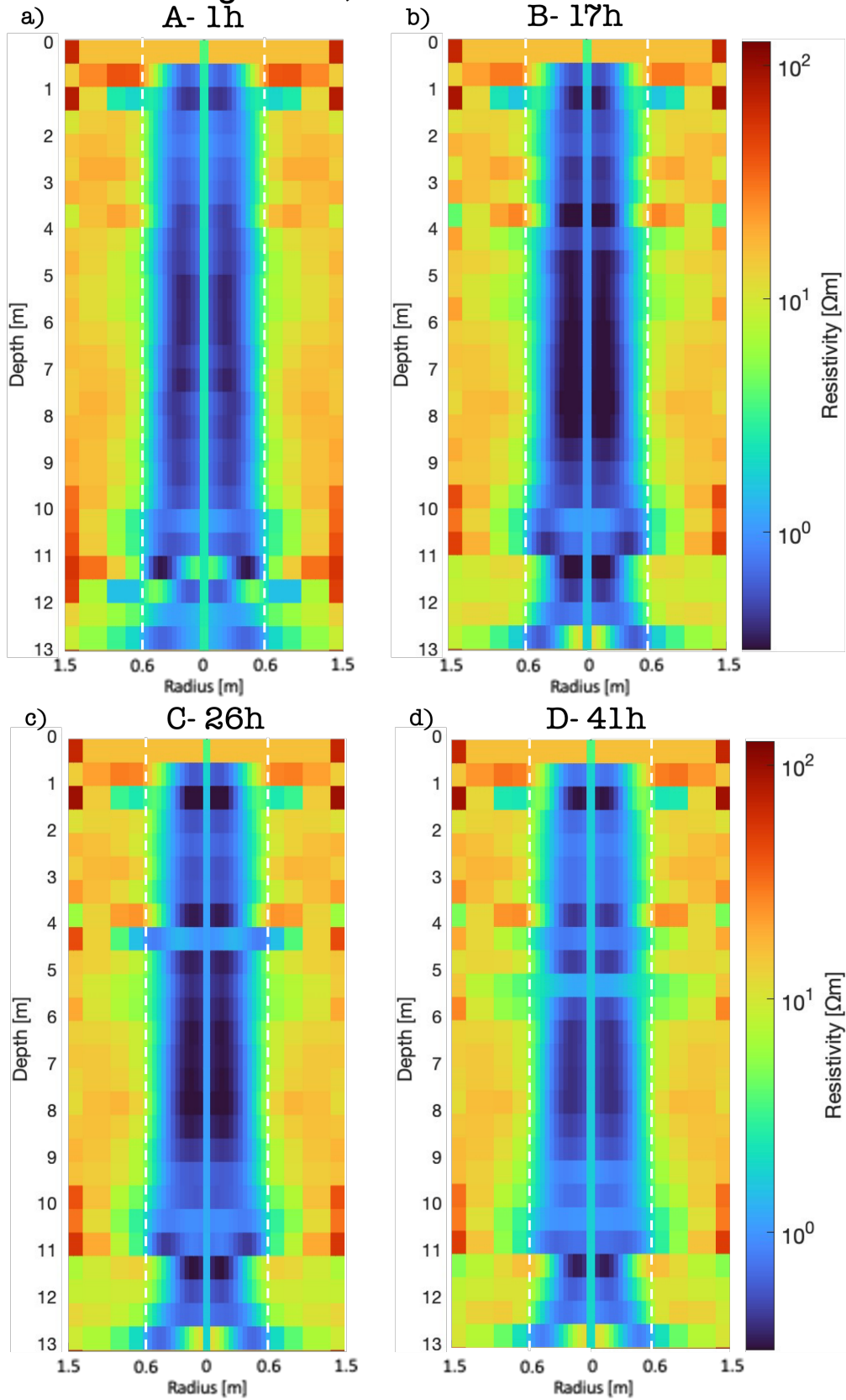


Figure 22 Multi-ring model, of the data from Moss. a) A, b) B, c) C and d) D are measurements taken after different times of curing. A, 1h; B, 17h; C, 26h; D, 41h. The dashed lines show the nominal diameter.

## Multi-ring model, measured data Moss

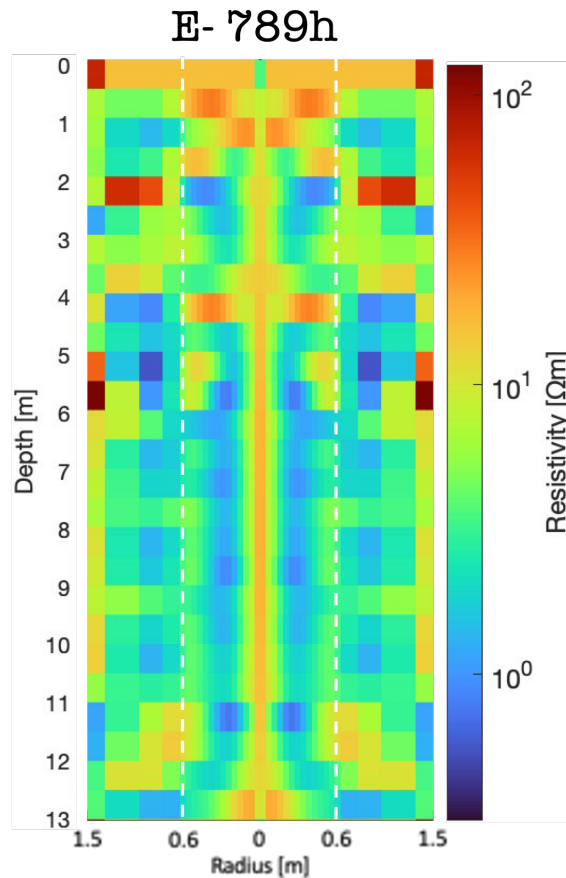


Figure 23 Multi-ring model, of the data from Moss. E are measurements taken after 789h of curing. The dashed lines show the nominal diameter.

### 5.3 Comparison of the jet grouted columns

Figure 24 and Figure 25 present the different inversions results of the measurements in Moss, with AarhusInv, Res2DInv and pyGIMLi. The two last mentioned are taken from Nilsagård & Knutsson (2022). The AarhusInv inversion results are from the multi-ring model. Note that the pyGIMLi results are single sided, where only the right half of the column is shown.

The inversion results based on the measurements after 1h of curing is shown in Figure 24a. In the inversion results from AarhusInv a section with a radius around 0.6 metres is shown. The resistivity for the section is around  $2 \Omega m$ . The intended column section in the Res2DInv, has a smaller radius than 0.6 metres and a higher resistivity than AarhusInv. The radius in pyGIMLi is smaller than 0.6 metres but the resistivity is similar to AarhusInv. There are some deviations in the results from Res2DInv where the vertical resistivity in the column section is not as cylindrical as in the other two inversion softwares. There is a transition zone in the pyGIMLi plot between the column and the surrounding subsurface. The center core, that is shown in the AarhusInv inversion results, is missing in the two other inversion results. The surrounding resistivity is similar in AarhusInv, Res2DInv and pyGIMLi with resistivity values between 10 and  $100 \Omega m$ .

The inversion results for the measurements after 17h of curing are shown in Figure 24b and after 26h are shown in Figure 25a. Similar conclusions as the once made on the results after 1h of curing time can be drawn of these two results. The inversion results based on measurements after 41h are shown in Figure 25b. Here, clear differences between the Res2DInv inversion and the other two softwares can be seen. The resistivity of the surrounding soil is much higher ( $>100 \Omega m$ ) for the Res2DInv results than for the others (10-50  $\Omega m$ ).

AarhusInv and pyGIMLi have small changes in resistivity and geometry by time, Res2DInv has high changes in resistivity by time. The resistivity of both the low resistivity column and the high resistivity surrounding subsurface is changing with time in Res2DInv. All of the three softwares inverted models have deviations in the subsurface ring at the first 0.5 metres of the column height, where the resistivity is higher than the rest of the column. These deviations is extra notable in the AarhusInv and the pyGIMLi inversions.

The relative resistivity changes in comparison to one hour of curing of the multi-ring model are shown in Figure 26, where the data is based on inversion results from the stabilized columns in Moss. The four models in the figure compare different times of curing, model A, 17h (a); B, 26h (b); C, 41h (c); D, 789h (d). The results of the comparison (Figure 26) are similar in model A, B and C. Where, the changes are equally spread over the model area with an increase of the column resistivity and a reduction of the surrounding soil resistivity. Model D shows similar results, but the resistivity is increasing and decreasing more, in the column and the surrounding soil, respectively, than in the previous models. Model E shows an increase of the center of the column section, while the same part is constantly decreasing in all the other models. It was not trivial to make a similar comparison of the few-ring model inversion results due to the large variations of the ring thicknesses from model to model.

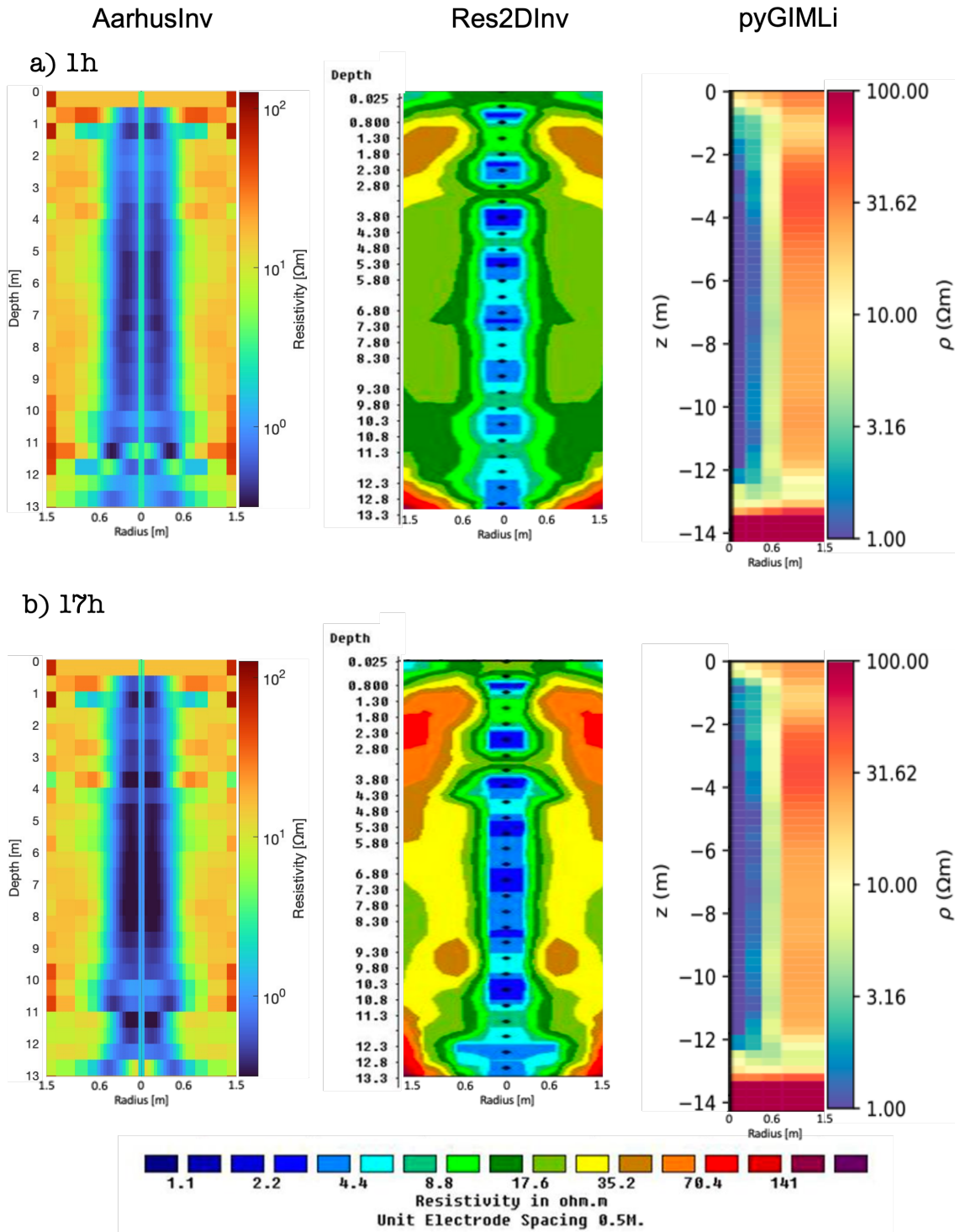


Figure 24 Comparison of inversions results of measured Moss data, inversions are done with; AarhusInv (left); Res2DInv (middle); pyGIMLi (single sided, right). a) data taken after 1h and b) data taken after 17h. Modified figures (Nilsagård & Knutsson, 2022).

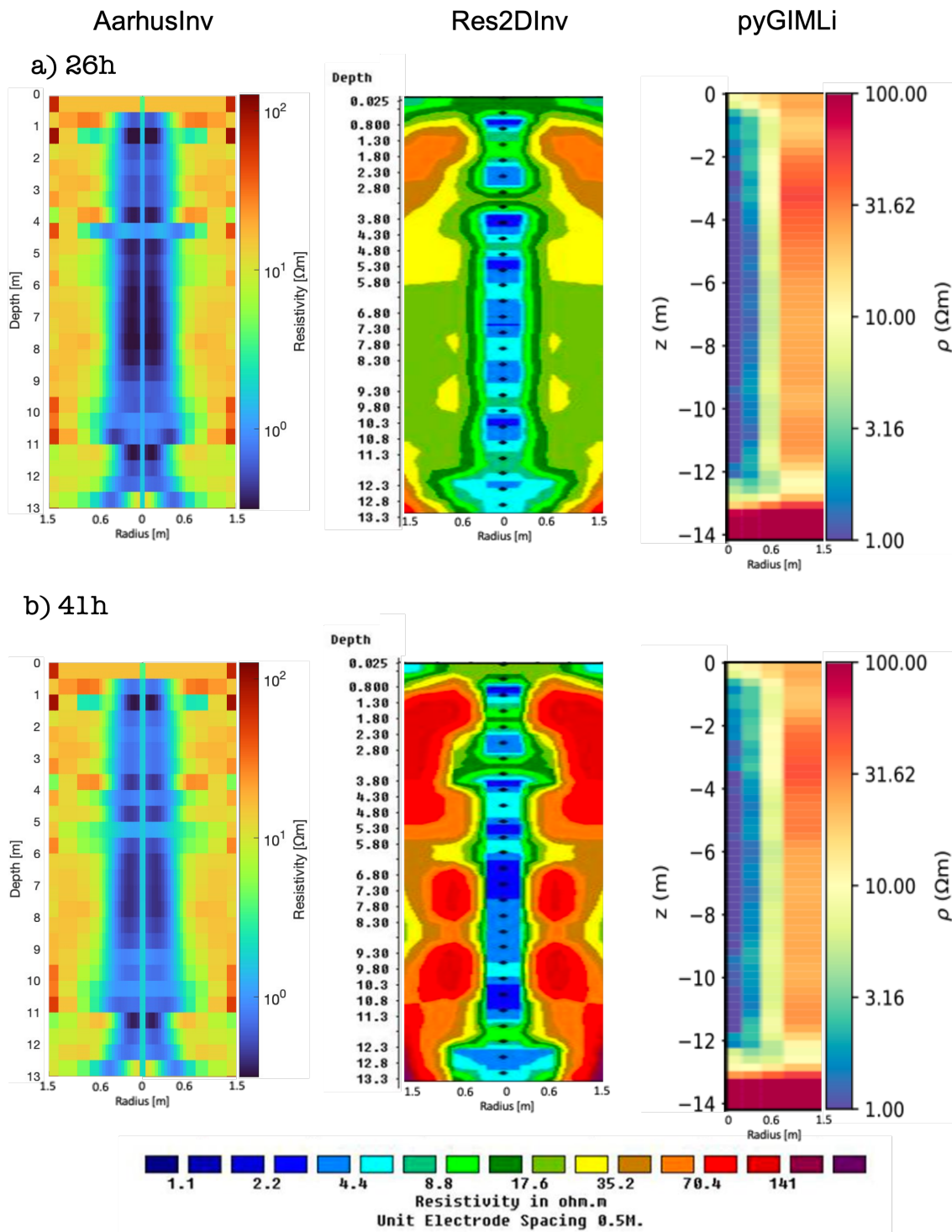


Figure 25 Comparison of inversions results of measured Moss data, inversions are done with; AarhusInv (left); Res2DInv (middle); pyGIMLi (single sided, right). a) data taken after 26h b) data taken after 41h. Modified figures (Nilsagård & Knutsson, 2022).

### Relative resistivity change of multi-ring model, in relation to one hour of curing

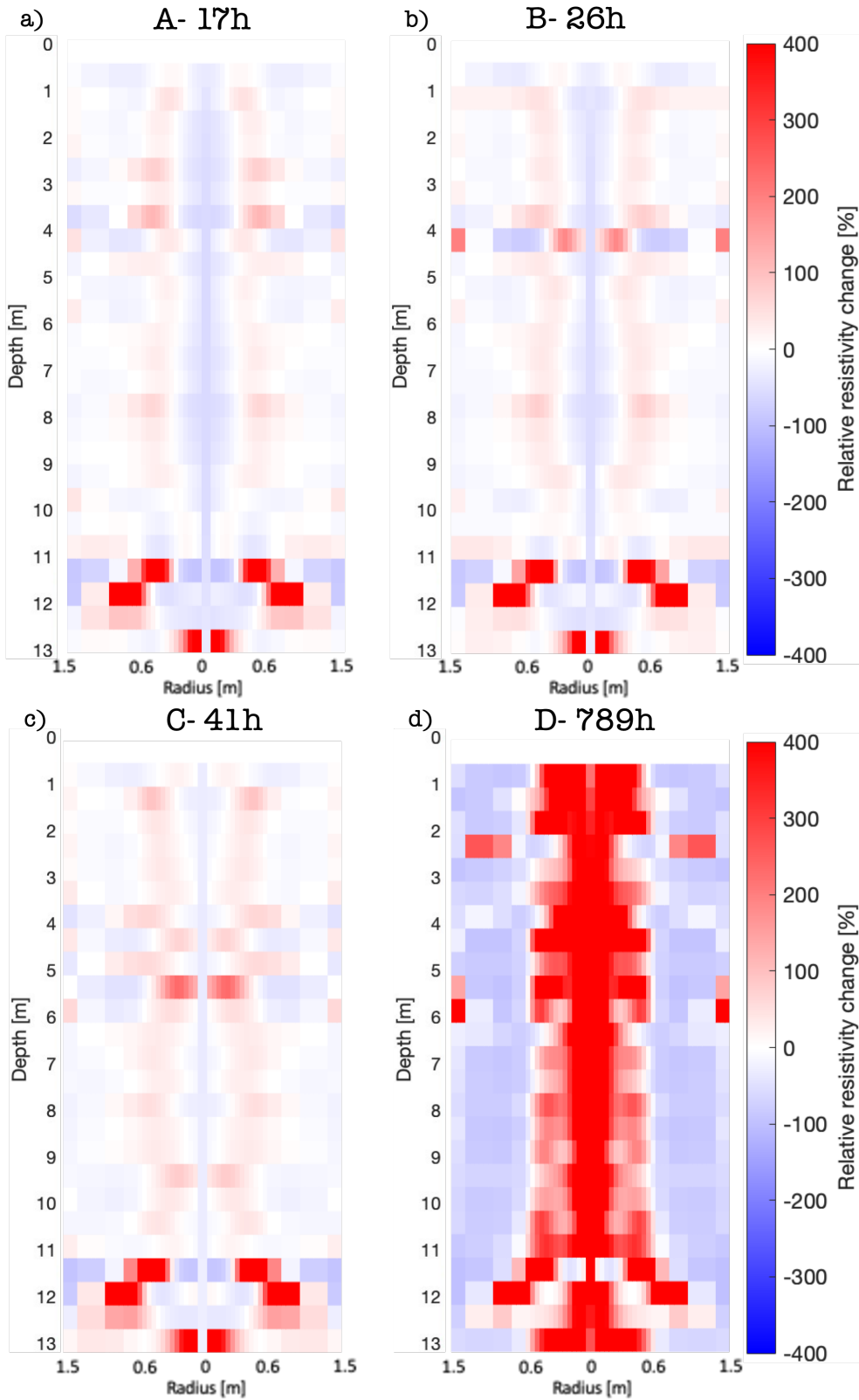


Figure 26 Relative resistivity change of the multi-ring model inversions in relation to the measurement performed after 1h of curing. The red regions are positive changes, and the blue regions are negative changes.

# 6 Discussions

The inversions performed on forward data give results with clear boundaries between the different rings. Both the few-ring and the multi-ring model match the designed geometry, except for the cases with a radius below 0.6 metres. The small radius part of the multi-ring model gives poor resolution and smooth correlations between the rings (Figure 18c & d) caused by a large contrast. The bad resolution of the small radius could probably be solved by using a denser electrode spacing. The few-ring inversions performed on models with an inserted part (see Figure 16c & d), gives a radius that is growing towards the middle or the bottom of the models. This could be explained in a similar way as for the multi-ring model by poor resolution and by the large difference between the starting model radius boundary and the measured data radius. It would be interesting to better match the starting model to the synthetic data geometry, but since the geometry of a real column is unknown that could become a second inversion. The second inversions starting model could be based on the first inversions results and by approaching the boundary of the low resistivity column. There is a high resistivity ring in the top 0-0.5 metres of both models. The ring has the same resistivity as the core and in the few-ring model it forms a disc, in the multi-ring model it is a ring with a resistivity higher than the core and more similar to the surrounding subsurface (see Figure 15 & 17). The rings recurrence and placement in the models is probably caused by the lack of electrodes placed over this surface layer.

The noise is generated according to Equation 3.22, where the noise percentage is taken from the mean between the minimum and the maximum resistivity value and then added to the resistivity. The percentage is randomly generated and normally distributed but due to only 27 electrodes, there may not be enough data points to make it normally distributed. Due to the large variations in resistivity, there is also a risk that the added resistivity value on low resistivity values results in very large errors. According to the presented results a noise level of 4 % or higher makes the results unreliable with bad resolution. This might have looked differently if the noise was based on the mean of all the resistivity values.

In comparison to the few-ring model, the multi-ring model inversion results of the synthetic data is less affected by the noise (see Figure 16 & 18). It is typical that the added noise makes the inverted few-ring model grow and the radius becomes larger than the design radius. This is probably because of the worse resolution in the few-ring model compared to the multi-ring model. The resolution in the few-ring model makes the boundaries also sharper.

The boundaries between the different rings in the few-ring model inversion results based on data from Moss is clear. The inversion results from the multi-ring model have more blurry boundaries. The blurry boundaries could be better suited to reality if there is a gradual transition zone between jet grouted column and the surrounding subsurface. The irregular geometry is expected, so (see Figure 2) this should also cause variations in resistivity. The models differ in length of the radius, where the mean length of the few-ring radius is slightly shorter. The explanation can be the non-sharp transmission zone between the column and the surrounding subsurface in the multi ring model. One advantage with the few-ring model is that it has a simpler design than the multi-ring model and may give a quicker overview than the more detailed multi-ring model. The inversion time and on computer is the same for these relatively small amount of data files. The case could be different for much larger quantities of data.

According to the site description, the surrounding subsurface of the column consists of quick clay. In Figure 5 it is shown that the resistivity of clay is in the span between 10 and 100  $\Omega m$ . According to Ranka, et al. (2004) the resistivities of the outer rings is in the span of a quick clay. The soilcrete in the jet grouted column is possibly shown as the low resistivity zone. And the center of the column, where the soilcrete was injected, is a medium resistivity zone with a slightly higher resistivity. Based only on the inversion results of the Moss data, it is not possible to know if the results are correct. To achieve certainty, the method needs to be validated. Validation of the method can be achieved for example by an excavation of the column which has not been done.

The inversion results from the measurements performed after 789 hours of curing in Figure 21 and Figure 23 shows a subsurface with column resistivities that are in the same range as the soil resistivities. It is possible that the resistivities of the columns have changed over the curing process of the soilcrete but it is unlikely that the resistivity of the surrounding subsurface has changed in that extent. Small changes of the soil resistivity could be expected due to the disturbance that is caused by the installation of the stabilized column. The extreme variations in resistivity compared to the earlier measurement times is probably caused by a combination of misalignment of the electrode cable and corrosive action on the electrodes surface (Nilsagård & Knutsson, 2022). The decrease of the soil and column resistivity could possibly be explained by a temperature increase, that is caused by installations of stabilised columns in the area where the measured column is located. It is also imaginable that the column is not fully cured when the last measurement was performed (Dahlin, et al., 2023).

The noise level of the measured data needs to be estimated. If the data is too noisy, it can result in an estimated column radius that is greater than the actual radius (according to the synthetic inversion results). The inversion results are based on measured data taken at different times after the injection. The last measurement taken after 789 hours of curing suffers from quality problems (Figure 21 & Figure 23). It would have been interesting to compare measurements on fully cured concrete with good resolution, to measure how the resistivity and geometry of the soilcrete develop over time.

Based on the inversion results, the radius of the column is mostly less than 0.6 meters. It is not possible to draw any conclusions on the column quality, due to the lack of knowledge on how the resistivity and the stiffness of the column develop further in time. But, based on the results and measurements from the first 41 hours it seems like the soilcrete consists of a homogenous mixture due to its relatively constant resistivity.

All the software's gives a mean radius below 0.6 metres. The inversion results from the pyGIMLi software gives a radius that appears to be smaller compared to AarhusInv and Res2DInv likely because of the gridding of the model has larger cells. The resistivity values of the surrounding soil and the jet grouted column are similar in AarhusInv and pyGIMLi. The centre core in the middle of the jet grouted column is only shown in AarhusInv. The core is expected and added to the model in AarhusInv with a fixed radius. Res2DInv has some built in structures (see Figure 24 & 25). The structures are placed in the column in the middle of the model. The structures make the models hard to interpret. The structures could be true due to Figure 2a that shows that the radius of a jet grouted column can vary a lot. The different look of the Res2DInv figures is also caused of its assumed non-cylindrical inversion geometry. The pyGIMLi inversion results have a poor resolution due to the chosen few layers but the surrounding resistivity and the column resistivity is matching AarhusInv. The inversion result from Res2DInv is not just mismatching the other two results, it is also changing a lot over time which is unreasonable since resistivity of the surrounding subsurface is not expected to change that much. The resistivity is also changing over time in AarhusInv and pyGIMLi but not to a great extent. Due to the curing of the soilcrete some variations of the physical properties over time is expected but maybe 789h is not long enough. The best resolution and model is obtained with AarhusInv, this is probably because of its ability to perform inversions with a cylindrical geometry.

The software AarhusInv is free to use for non-commercial purposes, Res2DInv is a paid program and pyGIMLi is a free open-source program. The best software to use in an economical and scientific perspective are therefore pyGIMLi and AarhusInv.

The comparison of different times in relation to one hour of curing (Figure 26) of the multi-ring model shows that the column resistivity is increasing and the surrounding soil resistivity is decreasing in all four comparisons. The most extreme changes are shown in the comparison with the measurements performed after 789h of curing. The increase of the column resistivity is probably an effect of the curing of the soilcrete and a reduced water content. The decrease of the surrounding soil resistivities are discussed earlier in this chapter.

The tables (Table 4- 7) with the residuals show that the noise is affecting the residual value in both the few-ring and the multi-ring model. With increasing noise with time, the residuals also increase. The residual value of the measured data model E (789h) is high in both inversion models. That was also expected because of the bad data quality of the last measurement. There are some deviations in the residuals to be commented. Firstly, the few-ring model of the synthetic data with 5% noise has a value that is lower than the rest of the noisy models, due to good inversion model fitting. Secondly, the few-ring model B and the multi-ring model D have a residual value that is higher than the rest of the residuals. The values are in both cases as high as the value of the model E. It was expected that the high residual should appear in the same place, since the inversions are based on the same measured data. The deviation of the residual could be a result caused by the differences between the two inversion models.

The results with AarhusInv have been inverted with a cylindrical geometry. A combination of the few-ring model and the multi-ring model could possibly create a well suited model of the column geometry. It would be interesting to use the few-ring model to create an overview of the geometry of the column due to its ability to vary the radius. The results of a previous inversion could be used to create a starting model for the inversion with geometry and resistivities that is better suited to the real column. The multi-ring model have 18 rings but it could be preferable to have even more rings to improve the resolution. The number of rings have to correlate with the number of data measured in the survey. A too large amount of model cell (rings) could instead worsen the resolution.

An advantage with the ERT method as a QC is that it is not as invasive to the jet grouted column and the surrounding subsurface as a caliper or an excavation. The composed measuring cable should not have any considerable effect on the column due to its relatively small cross-sectional area. The cable do not have any considerable effects on the mechanical properties of the column or the surrounding subsurface. Due to the small or even negligible effect on the surrounding subsurface, the ERT method can be used as a potential indirect quality control method.

# 7 Conclusion

The inversion of the cylindrical synthetic data shows that it is possible to invert cylindrical objects with varying radii in AarhusInv. Although there are some small deviations from the designed geometry, the inversion results mostly match the modelled geometry. Both a few-ring and a multi-ring inversion model work and give similar results. The results show that an increasing level of noise have a negative effect on the resolutions. Already a level of 4 % noise makes the inversion results unreliable.

The AarhusInv software inversion results of the Moss data show a subsurface cylindrical construction with a deviant resistivity compared to the surrounding subsurface. The subsurface column has an expected radius around 0.6 meter along most of the column. The radius of the inverted models is less than 0.6 meter. There is a distinct core in the middle of the column. The few-ring model and the multi-ring model give similar results. The inversion results show that 41 hours after injection, the radius of the jet grouted columns is less than the designed radius of 0.6 meters in parts of the column.

Compared to Nilsagård & Knutsson (2022), the AarhusInv inversion results are comparable to the results from pyGIMLi, due to the clear column shaped object. The two models show similar radii but due to the low resolution in the pyGIMLi inversion, the radius is easier to determine in the AarhusInv model. In contrast, a high increase of the resistivity of the surrounding soil is shown in the Res2DInv results.

The clear contrast in resistivities that have been found, make the ERT method a potential quality control method. The result of the control is strongly affected by noise. Thus, the measured data have to be well prepared before the inversion to be able to form a basis for any conclusions. The QC works on synthetic data but to be able to see how it works on measured data, a validation is needed.

## 7.1 Recommendations

The ERT method needs to be validated to be a QC method. It is recommended to perform the measurements on a jet grouted column and then excavate the column. The results from the inversion of the ERT measured data and the excavation can show the accuracy of the QC. It is recommended to use the AarhusInv and the few-ring model for the inversion due to the simple setup and clear results. The method can then be compared to other QC's.

The scope of this master thesis has been limited to the DC resistivity measurements. Since also the polarization properties can be measured and can give additional data, it is recommended to try to use induced polarization (IP) data or adding information about this kind of measurement to an inversion.

## 8 References

- Archie, G. E., 1942. The Electrical Resistivity Log as an Aid in Determining Some Reservoir Characteristics. Society of Petroleum Engineers, Volume 146(Issue 01), pp. 54-62.
- Auken, E. o.a., 2003. Piecewise 1D laterally constrained inversion of resistivity data, Aarhus: Geophysical Prospecting.
- Auken, E. et al., 2014. An overview of a highly versatile forward and stable inverse algorithm for airborne, ground-based and borehole electromagnetic and electric data. Csiro Publishing, 29 July, pp. 224-235.
- Auken, E., 2020. AarhusInv: Manual for the inversion program. 10.1 ed. Aarhus: HydroGeophysics Group.
- Bearce, R. G., Mooney, M. A. & Kessouri, P., 2016. Electrical Resistivity Imaging of Laboratory Soilcrete Column Geometry, s.l.: American Society of Civil Engineers.
- Bing, Z. & Greenhalgh, S., 2000. Cross-hole resistivity tomography using different electrode configurations. In: Geophysical Prospecting. s.l.:s.n., pp. 887-912.
- Binley, A. & Slater, L., 2020. Resistivity and induced polarization : theory and applications to the near-surface earth. Cambridge: Cambridge University.
- Carlsten, P., 1996. Lime and Lime/Cement Columns. In: S. G. Institute, ed. Embankments on Organic Soils. s.l.:Elsevier,, pp. 355-396.
- Croce, P., Flora, A. & Modoni, G., 2014. Jet Grouting. Boca Raton: Taylor & Francis Group.
- Dahlin, T. & Zhou, B., 2006. Multiple-gradient array measurements for multichannel 2D resistivity imaging, Lund, Adelaide: Near Surface Geophysics.
- Dahlin, T. o.a., 2023. Assert - Kvalitetskontroll av markstabilisering med elektrisk resistivitetstomografi (ERT), Lund, Linköping: LTH/Lunds universitet; SGI.
- Dazhi, W., 2005. Use of Jet Grouting in Deep Excavations. In: I. Buddhima & C. Jian, eds. *Ground Improvement — Case Histories*. Singapore: Elsevier, pp. 357-358.
- El-Shahat, A., 2017. *Electrical Resistivity and Conductivity*. West Lafayette: InTech.
- Keller Geoteknikk AS, 2023. *Keller*. [Online]  
Available at: <https://www.keller-geoteknikk.no/en/news/keller-geoteknikk-lands-eu42m-norway-contract>  
[Accessed 13 May 2023].
- Kirsch, K. & Bell, A., 2013. *Ground Improvement*. 3 ed. Boca Raton: Taylor & Francis Group.
- Larsson, R., 2006. *Djupstabilisering med bindemedelsstabiliserade pelare och masstabilisering*, Linköping: Swedish Deep Stabilization Research Centre.
- Loke, M., 1996. *Tutorial : 2-D and 3-D electrical imaging surveys*. s.l.:s.n.
- Naturvårdsverket, 2023. *Klimatet och bygg- och fastighetssektorn*. [Online]  
Available at:  
[https://www.naturvardsverket.se/amnesomraden/klimatostallningen/omraden/klimatet-och-bygg--och-fastighetssektorn/](https://www.naturvardsverket.se/amnesomraden/klimatomstallningen/omraden/klimatet-och-bygg--och-fastighetssektorn/)  
[Accessed 31 05 2023].
- Nicholson, P. G., 2015. *Soil Improvement and Ground Modification Methods*. Kidlington: Butterworth Heinemann.

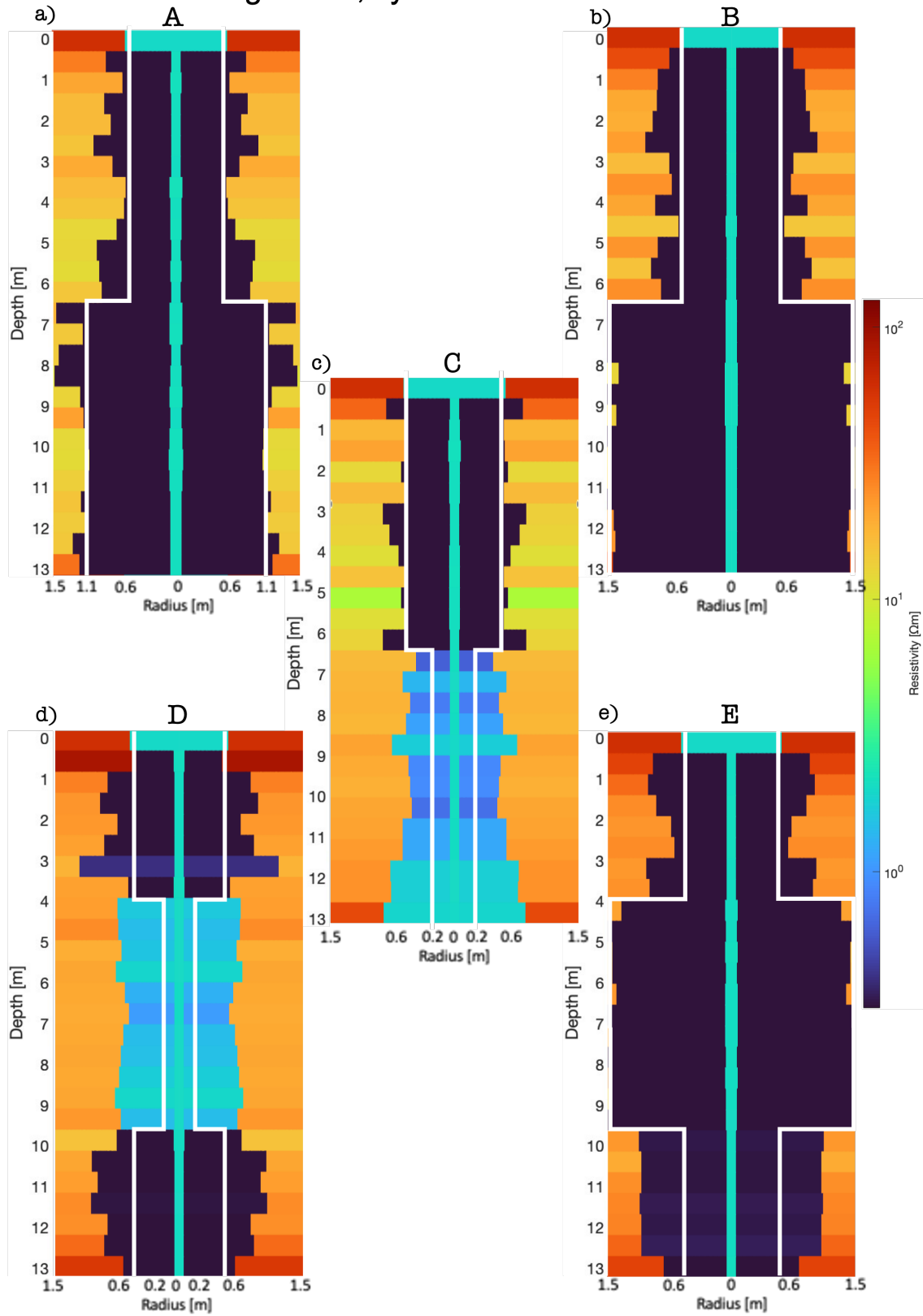
- Nilsagård, E. & Knutsson, R., 2022. *Application of ERT for Quality Assurance in Jet Grouting Columns*, Lund: Division of Engineering Geology, Faculty of Engineering, Lund University.
- Norges geologiske undersøkelse, 2023. *ngu.no*. [Online]  
Available at: <https://www.ngu.no/geologiske-kart>  
[Accessed 12 May 2023].
- Oldenburg, D. W., Kang, S. & Heagy, L. J., 2023a. Geophysical inversion for engineers. In: *Engineering Geophysics*. s.l.:Taylor & Francis, pp. 10-20.
- Oldenburg, D. W., Kang, S., Heagy, L. J. & Maxwell, M., 2023b. Direct current resistivity methods. In: *Engineering Geophysics*. Leiden: Taylor & Francis Group, pp. 67-75.
- Pädam, S., Balian, D., Uppenberg, S. & Wadström, E., 2021. *Klimatneutral betong genom kravställning*, Stockholm: Naturvårdsverket.
- Ranka, K. o.a., 2004. *Quick clay in Sweden*, Linköping: Swedish geotechnical institute.
- Roncicka, M., Günther, T., Grinat, M. & Wiederhold, H., 2020. Monitoring freshwater–saltwater interfaces with SAMOS – installation effects on data and inversion. In: *Near Surface Geophysics*. Hannover: European Association of Geoscientists and Engineers, pp. 333-463.
- Tsourlos, P., Kim, J.-H., Vargemezis, G. & Yi, M.-J., 2007. *Monitoring water injection with borehole ERT: preliminary results of an experiment carried out in Sindos (N. Greece)*, Thessaloniki: Aristotle University.
- Zhou, B., Bouzidi, Y., Ullah, S. & Asim, M., 2020. *A full-range gradient survey for 2D electrical resistivity tomography*, Abu Dhabi: Near Surface Geophysics.



# Appendices

# Synthetic data with 5% noise

## Few-ring model, synthetic data with 5% noise



# Multi-ring model, synthetic data with 5% noise

